
This is an electronic reprint of the original article.
This reprint may differ from the original in pagination and typographic detail.

Shukla, Monu Kumar; Kaushik, Harsh; Tiwari, Harshita; Behera, Chittaranjan; Tonk, Rajiv Kumar; Husain, Asif; Singh, Jay; Kesari, Kavindra Kumar; Kumar, Deepak

Development and characterization of *Myrica esculenta* plant extract-based albumin nanoparticles for anticancer activity

Published in:
Industrial Crops and Products

DOI:
[10.1016/j.indcrop.2024.118815](https://doi.org/10.1016/j.indcrop.2024.118815)

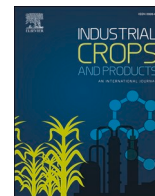
Published: 15/10/2024

Document Version
Publisher's PDF, also known as Version of record

Published under the following license:
CC BY

Please cite the original version:
Shukla, M. K., Kaushik, H., Tiwari, H., Behera, C., Tonk, R. K., Husain, A., Singh, J., Kesari, K. K., & Kumar, D. (2024). Development and characterization of *Myrica esculenta* plant extract-based albumin nanoparticles for anticancer activity. *Industrial Crops and Products*, 218, 1-20. Article 118815.
<https://doi.org/10.1016/j.indcrop.2024.118815>

This material is protected by copyright and other intellectual property rights, and duplication or sale of all or part of any of the repository collections is not permitted, except that material may be duplicated by you for your research use or educational purposes in electronic or print form. You must obtain permission for any other use. Electronic or print copies may not be offered, whether for sale or otherwise to anyone who is not an authorised user.



Development and characterization of *Myrica esculenta* plant extract-based albumin nanoparticles for anticancer activity

Monu Kumar Shukla^a, Harsh Kaushik^a, Harshita Tiwari^b, Chittaranjan Behera^c,
Rajiv Kumar Tonk^d, Asif Husain^e, Jay Singh^f, Kavindra Kumar Kesari^{g,h,*}, Deepak Kumar^{a,**}

^a Department of Pharmaceutical Chemistry, School of Pharmaceutical Sciences, Shoolini University, Solan, Himachal Pradesh 173229, India

^b Drug Chemistry Research Centre, Kanadia Road, Indore, Madhya Pradesh 452003, India

^c Department of Biotechnology, Guru Nanak Dev University, Amritsar, Punjab 143001, India

^d Delhi Pharmaceutical Sciences and Research University (DPSRU), Mehrauli-Badarpur Road, Pushp Vihar, Sector 03, New Delhi 110017, India

^e Department of Pharmaceutical Chemistry, SPER, Jamia Hamdard University, New Delhi 110062, India

^f Department of Chemistry, Institute of Science, Banaras Hindu University (BHU), Varanasi, Uttar Pradesh 221005, India

^g Department of Applied Physics, School of Science, Aalto University, Espoo 02150, Finland

^h University Centre for Research and Development, Chandigarh University, Mohali, Punjab 140413, India

ARTICLE INFO

Keywords:

Nanoparticulate formulation

Myrica esculenta

Bovine serum albumin

Anticancer activity

MIA PaCa-2 cell line

Drug delivery

ABSTRACT

Myrica esculenta plant extracts have been reported for their anticancer properties. Also, albumin has been reported as a drug carrier due to non-immunogenic nature and ability to bypass the reticuloendothelial system (RES). In this study *Myrica esculenta* plant extract-based albumin nanoparticles (ME-BSANPs) were characterized and prepared for cancer therapy. The objective of this study is to enhance the absorption of the phytoconstituents and to improve cancer cell selectivity that leads to apoptosis. The prepared nanoparticles were examined for their morphological characteristics, such as, size, shape, surface charge, and stability. Furthermore, the design of expert (DOE) software was used to determine the formulation parameters. The size of the synthesized nanoparticles were analyzed and images were observed in the field emission scanning electron microscopy (FESEM). *In vitro* studies of these nanoparticles were tested on cancer cell line (MIA PaCa-2) and resulted to cell cytotoxicity with an increase in the level of apoptosis or programmed cell death. The study of molecular docking was reported in *Myrica esculenta* bark. The docking was performed with BSA to check the binding affinity because BSA-based nanoparticles embedded with plant extract may interact with cancer targets. Docking studies revealed that the plant phytoconstituents have good binding affinity to BSA, which may carry these nanoparticles to target the cancer site to trigger apoptosis. These research findings suggest that the plant extract-loaded albumin-based nanoparticles could be a new development in cancer treatment. Also, these nanoparticles showed an excellent drug delivery and anticancer activities with fewer side effects.

1. Introduction

Pancreatic cancer continues to be among the most dreadful malignancies due to its dismal prognosis and meager survival rate, even with several breakthroughs in detection, surgical, radiation, and chemotherapy techniques (Xu et al., 2016). The majority of patients suffered from advanced localized or metastatic tumors, which may have contributed to the poor prognosis of the illness. Under these circumstances, patients with advanced-stage localized tumors have a typical

survival of 6–10 months, but the median survival time for those with metastatic cancer is just three to six months (Witjes et al., 2021; Shukla et al., 2022). There are many phytochemicals in *Myrica esculenta*, commonly known as Bayberry and has medicinal properties in the production of nanoparticles. The main bioactive phytoconstituents of this plant are myricetin, ellagic acid, caffeic acid, chlorogenic acid, gallic acid, threonine, ascorbic acid, furfural, and catechin, as seen in Fig. 1 (Sood and Shri, 2018).

Albumin, a biocompatible protein, as a carrier matrix underscores

* Corresponding author at: Department of Applied Physics, School of Science, Aalto University, Espoo 02150, Finland.

** Corresponding author at: Department of Pharmaceutical Chemistry, School of Pharmaceutical Sciences, Shoolini University, Solan, Himachal Pradesh 173229, India.

E-mail addresses: kavindra.kesari@aalto.fi, kavindra_biotech@yahoo.co.in (K.K. Kesari), guptadeepak002@gmail.com (D. Kumar).

<https://doi.org/10.1016/j.indcrop.2024.118815>

Received 16 February 2024; Received in revised form 15 May 2024; Accepted 20 May 2024

Available online 16 June 2024

0926-6690/© 2024 The Author(s). Published by Elsevier B.V. This is an open access article under the CC BY license (<http://creativecommons.org/licenses/by/4.0/>).

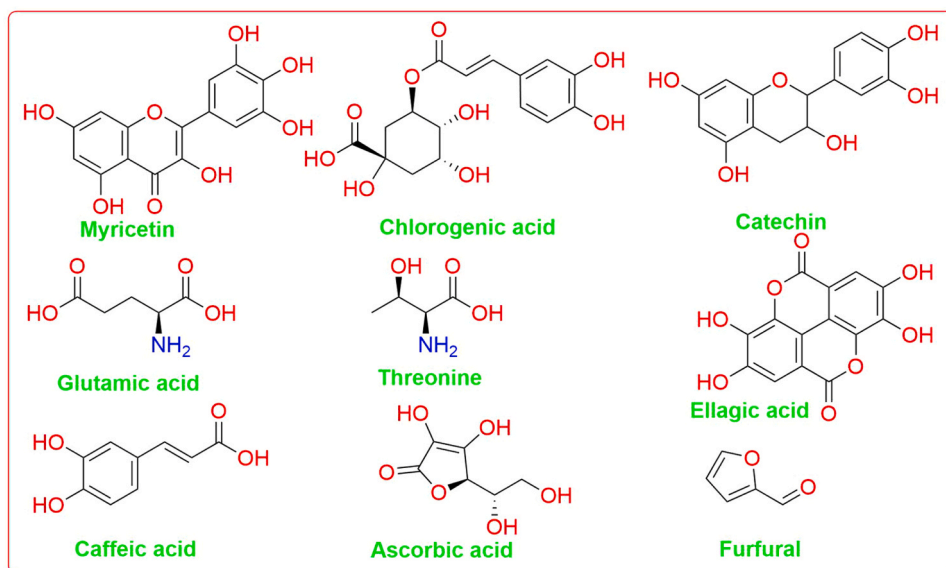


Fig. 1. Reported bioactive phytoconstituents of the plant *Myrica esculenta*.

the quest for sustainable and eco-friendly drug delivery systems. This research seeks to amalgamate the ancient wisdom of traditional medicinal plants with cutting-edge nanotechnology to forge a novel bio-nanoconjugate system with the ultimate goal of revolutionizing the landscape of anticancer treatments. A combination of cutting-edge technology in bio-nanoconjugation may develop unique methods especially for the cancer treatment (Shukla et al., 2022; Shukla et al., 2022).

In recent years, *Myrica esculenta* (ME) plant extract has been reported for the treatment of cancer and other related diseases (Saini et al., 2013; Bhatt et al., 2023; Shukla et al., 2023; Shukla et al., 2023), along with the development of nanoparticles (Chauhan et al., 2023; Shukla et al., 2023), and various metal-based nanoparticles (Fuku et al., 2016; Matinise et al., 2017; Hassan et al., 2018; Chauhan et al., 2020; Das et al., 2020; Maheshwaran et al., 2020; Sone et al., 2020; Sackey et al., 2020; Dhatwalia et al., 2023; Kumari et al., 2023; Verma et al., 2023). Albumin has gained a lot of interest in nanotechnology as a drug delivery strategy, especially for cancer treatment. It is a biocompatible, biodegradable, non-immunogenic, and non-toxic (Elzoghby et al., 2012; Behera et al., 2024). Moreover, it is a water-soluble protein that can tolerate temperatures as high as 60 °C for up to 10 hours and is stable across a broad pH range (Kratz, 2008). Additionally, it has carboxylic and amino groups that may utilize to modify the surface of nanoparticles. Targeting cancer cells is a key objective of cancer treatment to reduce side effects while also achieving selective drug accumulation in tumor tissues.

The rationale behind this research work is to deliver phytochemicals of ME extract, which include targeting cancer cells without harming normal cells as they are phytoconstituents and BSA causes selective drug accumulation in tumor tissues, which may improve therapeutic efficacy, reduce toxicity, and prevent drug resistance. This investigation aims to develop development and characterize *Myrica esculenta* plant extract-based albumin nanoparticles for their potential application in anticancer therapy. Using a desolvation process, methanolic ME extract has been loaded in BSA to prepare nanoparticles (ME-BSANPs). Numerous metrics, including size, polydispersity, zeta potential, and morphological characteristics, were evaluated for the ME-BSANPs. The cytotoxic potential of ME and ME-BSANPs were assessed using HEK-293 sparing normal cells and the MIA PaCa-2 cell lines. The developed formulations were examined to see how simple plant extract and the nanoparticles' cytotoxic activity correlated.

2. Materials and methods

2.1. Materials

Myrica esculenta plant bark collected from the Himalayan region of Solan district, Himachal Pradesh, India. Amphotericin B solution and MTT dye were bought from Sigma Chemicals, U.S.A., Alfa Aesar (England), Merck (India), and GIBCO Invitrogen Corporation provided fetal bovine serum (FBS), methanol, and 25% glutaraldehyde. We purchased 4% paraformaldehyde solution and bovine serum albumin (BSA) from Hi-Media in India.

2.2. Extraction of plant

Myrica esculenta barks were adequately cleaned and shade-dried for 15 days. Shade-dried barks were coarsely pulverized using a mortar pestle and a grinding machine. In Soxhlet's extractor (continuous hot percolation process), 250 g of powdered plant material was extracted with petroleum ether (60–80 °C) to remove lipids and waxes, then with methanol. After comprehensive extraction, the methanolic extract was concentrated under decreased pressure at 50–55 °C. The solvent was extracted using a rotary evaporator (Heidolph) at 40 °C in a vacuum. Dried extracts were stored in sealed containers at 2–4 °C for further use. This extract has been used for the preparation of nanoparticles in this study (Ahmad et al., 2022).

2.3. Preparation of ME-BSANPs

With a few modification, developing *Myrica esculenta* bark extract-based albumin nanoparticles (ME-BSANPs) were prepared according to the schematic illustration (Fig. 2) (Sand et al., 2015; Zinger et al., 2019; Saneja et al., 2019). Briefly, the desolvation process was used to prepare nanoparticles. The BSA solution was primarily prepared by stirring 40 mg of BSA in 2 ml of purified water using a magnetic stirrer. Further, 0.2 M NaOH raised the solution's pH approximately between 8 and 9. At room temperature, the solution was continuously stirred at 700 rpm. A syringe was used to dissolve the required amount of plant extract in methanol, which was then added dropwise (0.5 ml per minute) to the aqueous medium until turbidity was apparent.

The particles were then cross-linked with 1.175 µl of 8% glutaraldehyde per mg of BSA. Thereafter kept at ambient temperature and stirred magnetically at 700 rpm until the methanol had evaporated. The

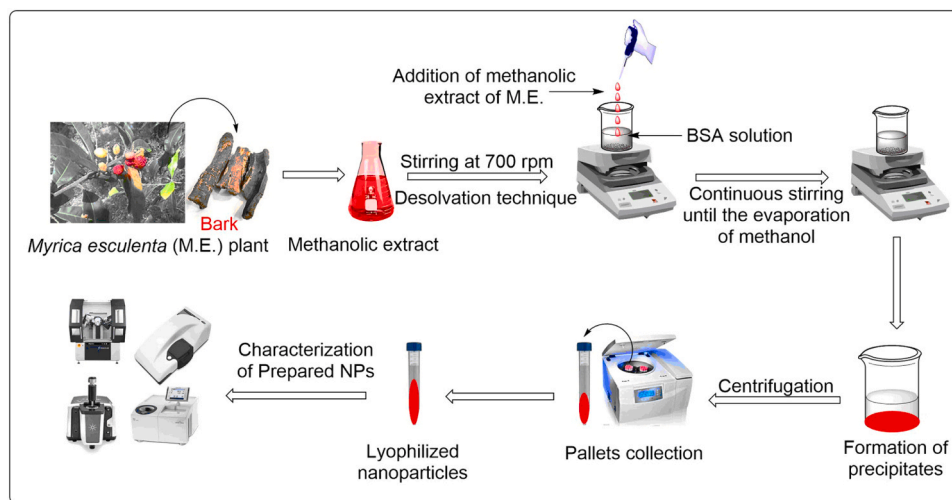


Fig. 2. A flowchart that represents the preparation of *Myrica esculenta* based BSA-NPs (ME-BSANPs).

nanoparticles were collected by centrifugation (12,000 rpm, 30 min) after the methanol evaporated. After three repeated washing, the nanoparticles were free of any remaining residues of methanol or glutaraldehyde and reconstituted with distilled water to a tenth of their initial volume. Thereafter, 5% sucrose was used to cryoprotect the nanoparticles during the freeze-drying process (VirTis, USA).

2.4. Optimization of formulation

Response surface methodology (RSM) is used to study complex multivariable systems and investigate how independent variables (factors) interact with one another and affect dependent variables (responses) (Haider and Soni, 2022). A quadratic model based on the Response Surface Methodology (RSM) and a randomized Box-Behnken design was used in the study. Design-Expert® Software version 10 by Stat-Ease Inc. was used to analyse the data. Each block had five center points. Compared to a three-level factorial design, the BBD model required fewer trials and offered designs with desirable statistical properties. It was developed using Design-Expert® Software version 10 (Stat-Ease Inc., MN). A quadratic model represented by the numbers -1, 0 and +1 is expressly accommodated by BBD, which has three levels for each component. In this study, "ME: ME-BSANPs (A)," "Stirring time (B)," "Stirring speed (C)," and "Sonication time (D)" were chosen as independent variables (factors) to look at three-dimensional (3D) response surface and see how they affected dependent variables (responses) like particle size (MPS) (R1), zeta potential (R2), and polydispersity index (R3). The experimental design comprised twenty-nine runs based on the model, creating various variable combinations using three components and three design levels, as detailed in Table 1. The coded and decoded values for all are summarized in Table 2. Data sets underwent ANOVA, with a significance level set at $p \leq 0.05$ in the surface response analysis.

Table 1

The optimization of the nanoparticles is based on factors (an independent variable), levels (+1, 0 and -1), and responses (dependent variables) according to RSM-BBD.

Factors	Levels		
	Low (-1)	Medium (0)	High (+1)
A: ME: ME-BSANPs ratio	0.1	0.55	1
B: Stirring time (min)	30	45	60
C: Stirring speed (rpm)	700	900	1100
D: Sonication time (min)	10	20	30
Responses	Constraints		
R1: Particle Size (nm)	Minimum		
R2: Zeta potential (mV)	In range		
R3: Polydispersity index (PDI)	In range		

Eq. 1 illustrates 15 polynomial coefficients in total (β_0 to β_{14}) derived from the specific mathematical modeling, where β_0 functions as the intercept.

$$Y = \beta_0 + \beta_1X_1 + \beta_2X_2 + \beta_3X_3 + \beta_4X_4 + \beta_5X_1X_2 + \beta_6X_1X_3 + \beta_7X_1X_4 + \beta_8X_2X_3 + \beta_9X_2X_4 + \beta_{10}X_3X_4 + \beta_{11}X_1^2 + \beta_{12}X_2^2 + \beta_{13}X_3^2 + \beta_{14}X_4^2 \quad (1)$$

In this formula, Y represents the observed outcome associated with each combination of factor levels. The coefficients β_1 , β_2 , β_3 , and β_4 correspond to the linear effects, while the interaction effects among the three factors are expressed by β_5 , β_6 , β_7 , β_8 , β_9 , and β_{10} . Moreover, β_{11} , β_{12} , β_{13} , and β_{14} are indicative of quadratic effects derived from the experimental data. The independent variables are denoted as X_1 , X_2 , X_3 , and X_4 .

2.5. Morphological analysis

The morphology and elemental content of plain ME extract and ME-BSANPs were examined using field emission scanning electron microscopy (FESEM) with energy-dispersive X-ray spectroscopy (EDS) techniques. For FTIR analysis, BSA (HK1), ME plant bark extract (HK2), physical mixture (ME extract and BSA) (HK3), and ME-BSANPs (HK4) were compressed using KBr to obtain thin pellets. Then, scanning of pellets was done in a range of 4000–400 cm^{-1} , and the spectra were recorded by Spectrum RXI FTIR (Perkin Elmer, USA). 2 mg of ME NPs and ME-BSANPs were taken for the FTIR analysis. The powder X-ray diffraction pattern of BSA (HK1), ME NPs (HK2) and ME-BSANPs (HK3) was studied by X-ray diffractometer (PAN analytical, X'Pert3 Powder, Netherlands). The operating voltage was 40 kV, the operating current was 25 mA, the start angle 2θ was 5° , and the finishing angle was 50° (Vivek-Ananth et al., 2023).

2.6. In vitro cell culture experiment

2.6.1. Maintenance of cell lines

Dulbecco's modified Eagle's medium-high glucose (DMEM), a complete growth medium, was used to cultivate the MIA PaCa-2 cell line with pen-strep and amphotericin-B solution in a humidified carbon dioxide incubator (ESCO) at 37°C , T75 culture flasks with 5% CO_2 and 95% relative humidity were used to cultivate the cells. To get a single-cell suspension, monolayer cell culture was performed, and cell harvesting was executed using a 0.25% (w/v) trypsin/EDTA (1 mM) solution. MIA PaCa-2 cells were in flat-bottom 96-well plates at the ideal cell density. The cell density per well used in this preliminary screening

Table 2

Factors and levels of ME: ME-BSANPs, stirring time, stirring speed and sonication time, and responses of MPS (nm), ZP (mV) and PDI according to the plan using RSM-BBD for nanoparticles.

Std	Run	Factor 1 A:ME: ME-BSANPs Ratio	Factor 2 B: Stirring time mins	Factor 3 C: Stirring speed rpm	Factor 4 D: Sonication time min	Response 1 Particle size nm	Response 2 Zeta potential mv	Response 3 PDI
16	1	0.55	60	1100	20	229.9	-17.3	0.52
27	2	0.55	45	900	20	256.5	-20.5	0.26
13	3	0.55	30	700	20	295.4	-24.9	0.51
5	4	0.55	45	700	10	272.1	-23.4	0.32
1	5	0.1	30	900	20	265.2	-32.5	0.34
2	6	1	30	900	20	400.4	-21.5	0.73
14	7	0.55	60	700	20	240.2	-17.8	0.68
9	8	0.1	45	900	10	256.4	-27.5	0.16
18	9	1	45	700	20	358.4	-18.9	0.81
29	10	0.55	45	900	20	254.6	-19.2	0.25
4	11	1	60	900	20	305.4	-13.3	0.9
7	12	0.55	45	700	30	264.2	-21.3	0.3
23	13	0.55	30	900	30	282.3	-24.2	0.41
20	14	1	45	1100	20	322.9	-15.5	0.66
10	15	1	45	900	10	345.4	-17.2	0.74
11	16	0.1	45	900	30	253.5	-26.3	0.3
19	17	0.1	45	1100	20	253.2	-27.5	0.28
28	18	0.55	45	900	20	251.2	-20.6	0.28
22	19	0.55	60	900	10	240.2	-17.8	0.6
26	20	0.55	45	900	20	255.2	-19.8	0.27
25	21	0.55	45	900	20	256.4	-19.4	0.26
6	22	0.55	45	1100	10	251.2	-18.9	0.21
12	23	1	45	900	30	339.3	-16.4	0.47
17	24	0.1	45	700	20	258.9	-28.4	0.32
24	25	0.55	60	900	30	238.4	-16.2	0.53
8	26	0.55	45	1100	30	248.4	-18.3	0.21
3	27	0.1	60	900	20	248.3	-22.6	0.44
15	28	0.55	30	1100	20	279.4	-23.7	0.37
21	29	0.55	30	900	10	283.3	-23.5	0.31

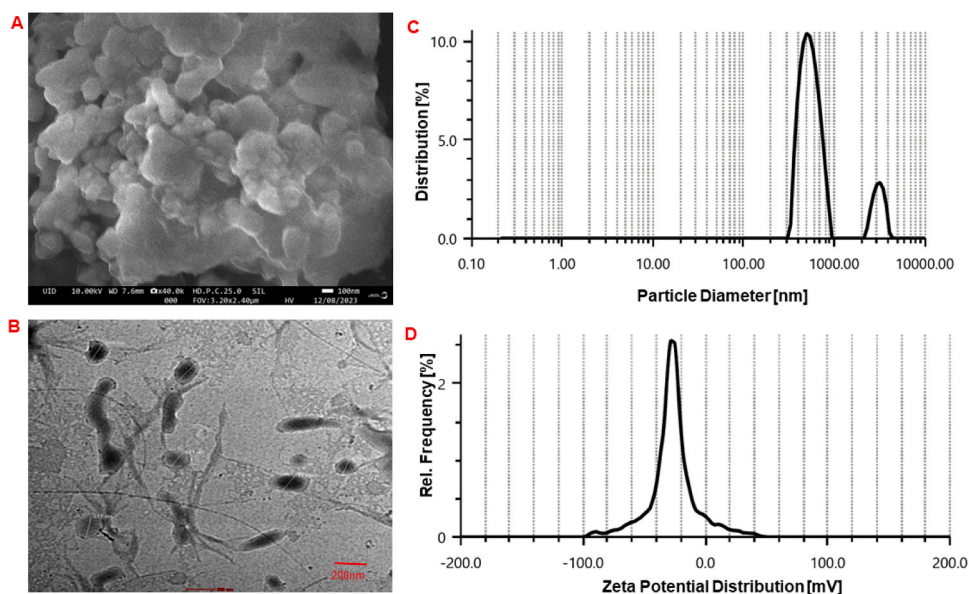


Fig. 3. Morphological characterization of prepared ME-BSANPs. A) FESEM image at 100 nm, B) TEM image at 200 nm, C) particle size distribution and D) Zeta potential of prepared nanoparticles.

procedure for the selected cell line was 7500. The MIA PaCa-2 cell line was procured from ATCC. With the MTT test, the *in vitro* anti-proliferative investigation was conducted.

2.6.2. Cell viability using MTT assay

MTT assay was used to quantify the cytotoxicity of the plain ME extract (HK1) and ME-BSANPs (HK2). In short, 96-well plates were seeded with 100 μ l/well cell suspensions of MIA PaCa-2 cells, which were then incubated for a whole day. MIA PaCa-2 cells were treated with

prepared samples of HK1 and HK2 at a concentration 1 μ g/ml each for 48 h for cytotoxicity evaluation. Camptothecin (0.25 μ g/ml) was used as a standardized positive control. Before termination of the experiment, the cells were exposed to MTT dye for four hours (2.5 mg/ml in PBS solution). After incubation, the insoluble formazan crystals were dissolved using DMSO (150 μ l) added to each well. And finally, the resulting-coloured solution was quantified using an ELISA microplate reader at 570 nm. Moreover, the percentage of cell viability compared to the control was calculated using the following formula IC50 values were

calculated using Graph Pad Prism 6.0. All experiments were performed in triplicates (n=3).

$$\% \text{cell viability} = \frac{(\text{Abs of test sample} - \text{Blank})}{(\text{Abs of Control} - \text{Blank})} \times 100$$

$$\% \text{cell growth inhibition} = 100 - \% \text{cell viability}$$

2.6.3. Cell viability analysis of normal cells

The cell viability of normal cells was evaluated using a Trypan blue exclusion assay. The dye Trypan blue helps in distinguishing the live versus dead cells and is easily countable using a hemocytometer under a bright field microscope. After the treatment with plain ME extract (HK1) and ME-BSANPs (HK2), cells were collected after trypsinization, pelleted down by centrifugation, and the pellet was again re-suspended in PBS (500 μl). An equal volume of trypan blue dye was mixed with an equal volume of cell suspension (1:1 ratio; 10 μl of trypan blue and 10 μl of cell suspension), mixed properly, and the number of cells was counted using a hemocytometer under a bright field microscope (100X magnification). Upon observation, the viable cells remain unstained, while the non-viable cells are stained blue and clearly differentiated. Cell viability is represented as the percent viable cells out of the total number of cells and calculated according to the method described previously (Section 2.6.2) (Behera et al., 2022).

2.7. Molecular docking studies

This study aimed to identify phytochemicals present in *Myrica esculenta* through the IMPPAT database, resulting in the identification of 55 phytoconstituents. All compounds underwent energy minimization and were converted to pdbqt format using OpenBabel integrated with the PyRx module, employing the universal force field and conjugated gradient method for 200 steps (Dallakyan and Olson, 2015; O'Boyle et al., 2011). A molecular docking simulation study was conducted on the Bovine Serum Albumin (BSA) receptor. The three-dimensional (3D) crystal structures of BSA (entry code 4F5S) were sourced from the Protein Data Bank (PDB), and the UCSF-Chimera DockPrep module was employed to prepare the protein structure (Pettersen et al., 2004; Bujacz, 2012). This involved removing heteroatoms and solvents from the PDB file, adding hydrogen atoms to correct the ionization and tautomeric status of amino acids, and incorporating charges using the CHARMM force field. Subsequently, the protein was loaded into the PyRx software and converted to pdbqt format. Molecular docking was performed using AutoDock Vina (version 4, The Scripps Research Institute, USA) within the PyRx platform, employing a blind docking approach to achieve the best binding pose (Trott et al., 2010). The grid dimensions were manually adjusted to cover the entire protein, with the following values: X (43.43), Y (56.19), Z (51.99), and center coordinates X (57.67), Y (4.11), Z (-22.56). After completing molecular docking, the docked complexes' poses were visualized using Maestro, a molecular modeling software by Schrödinger. Since the poses were originally in pdbqt format, which was incompatible with Maestro, they were converted to PDB format using Open Babel, a free chemical file format converter.

2.8. Statistical analysis

The data is shown as mean \pm standard deviation (SD). Individual group comparisons, multiple one-way ANOVA, and the Student's t-test were used for the statistical analysis of the data in order to compare groups. A statistically significant difference was defined as a p-value less than 0.05.

3. Results and discussion

3.1. Development of ME BSA-based nanoparticles

A desolvation technique has been used to develop bovine serum

albumin-coated methanolic extract of *Myrica esculenta* bark nanoparticles (ME-BSANPs). These prepared nanoparticles have been characterized using various modern techniques.

3.2. Surface morphology evaluation of the developed nanoparticles

EDS, along with FESEM and TEM, are typically used for elemental composition surveys. The developed ME-BSANPs exhibited spherical morphology when observed under FESEM and TEM. The prepared size in FESEM and TEM were found to be 547.9 nm and 160–222 nm respectively, and the polydispersity index (PDI) of the ME-BSANPs was found to be 24.1%.

The mean zeta potential of the prepared nanoparticles was -26.2 mV. The size of the nanoparticles, as seen in the TEM and FESEM, matched the size determined by dynamic light scattering (Fig. 3). An EDS graph of prepared ME-BSANPs was also performed, which showed the presence of carbon and oxygen elements (Fig. 4).

To find out the existing interaction between the plant phytoconstituents and the BSA, Fourier-transform infrared (FTIR) spectroscopy was used. The FTIR spectra of the plain BSA (HK1), methanolic ME bark extract (HK2), physical mixture of ME bark extract and BSA (HK3), and ME-BSANPs (HK4) have been included in the Fig. 5, which demonstrates different functional groups that attach to BSA's surface (Table 3). The phenolic, alcoholic, and surface-adsorbed H₂O hydroxyl groups may be responsible for the O-H stretching vibrations linked to the infrared (IR) bands detected in the 3300–3600 cm^{-1} regions.

Both symmetric and asymmetric CH₂ stretching are linked to the bands in the 2800–2900 cm^{-1} range. The bands corresponding to the C=O stretching vibrations range from 1550 to 1650 cm^{-1} . The bending vibrations of the -OH groups are attributed to the IR bands about 1398 and 1440 cm^{-1} . The stretching vibrations of C-O and C-C cause the presence of the infrared bands in the range of 1290–850 cm^{-1} . The ME of *Myrica esculenta* bark's FTIR spectra, show several functional groups in the extract. The FTIR spectra of the plant extracts and ME-BSANPs make it clear that NPs have more functional groups linked to the ME extract than the BSANPs.

Fig. 1 illustrates the bioactive compounds found in *Myrica esculenta* extracts, which include furfural, ascorbic acid, threonine, gallic acid, ellagic acid, caffeic acid, chlorogenic acid, and catechin. This makes it easier to see how the NPs convert.

Differential scanning calorimetry (DSC) has been performed to check the nature of compounds in the plant extract. DSC of plain BSA (HK1), methanolic ME bark extract (HK2), physical mixture of ME extract and BSA (HK3), and ME-BSANPs (HK4) have been depicted in Fig. 6. The thermal gravimetric analysis showed four significant steps of thermal decomposition with an overall weight loss of about 15.15% HK4. The first step, weight loss of \sim 3.3% up to 150 $^{\circ}\text{C}$ can be associated with the exclusion of physisorbed water and organic moieties from the NP surface.

The XRD patterns of plain BSA (HK1), methanolic ME bark extract (HK2), and ME-BSANPs (HK3) were depicted in Fig. 7, to study the characteristics of plant extract entrapped in the bovine serum albumin-based nanoparticles. The conspicuous peaks formed by diffraction at $2\theta = 27.6^{\circ}$, 38.2° , 43.5° , 54.3° and 81.6° . The crystalline nature is confirmed by the firm diffraction peaks of the plain BSA (HK1), methanolic ME bark extract (HK2), and ME-BSANPs (HK3).

3.3. RSM & BBD-based optimization

The Box-Behnken design (BBD) is a key tool in our research, facilitating the generation, formulation, and optimization of nanoparticle formulations. These formulations, labeled as Run 1 to Run 29, were subjected to a comprehensive evaluation for response variables, including Particle Size (PS) (R1), Zeta Potential (ZP) (R2), and Polydispersity Index (PDI) (R3). The design incorporated specific formulation factors: 'ME: ME-BSANPs (A),' 'Stirring time (B),' 'Stirring speed

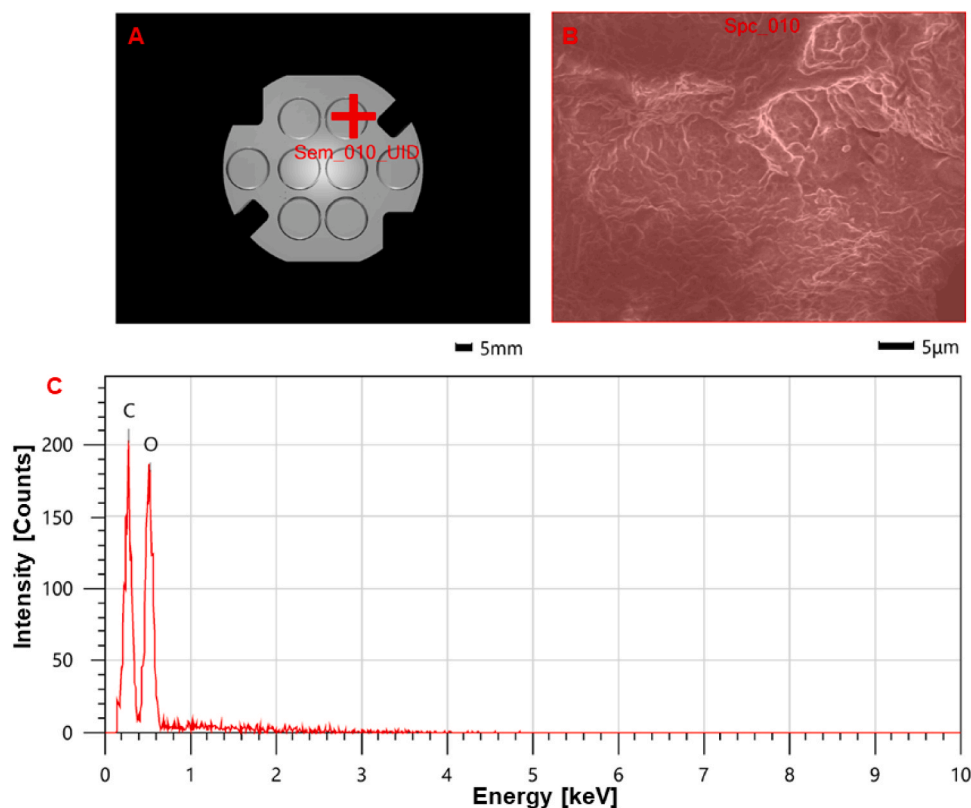


Fig. 4. EDS of prepared ME-BSANPs. A) Sample image, B) FESEM UID for EDS and C) EDS graph of prepared nanoparticles which showed the presence of carbon and oxygen elements.

(C), and 'Sonication time (D).' The resultant polynomial coefficients were derived from the quadratic polynomial model outlined in Eqs. 2, 4 and 5. This model was designed to investigate potential significant interactions between the responses, thereby enhancing our understanding of the nanoparticle formulation process.

The 3D response surfaces for particle size (PS) are shown in Fig. 8. PS's shed-like structure shows that the number of ME-BSANPs and PS are directly correlated. PS exhibits a linear rise when the number of ME-BSANPs goes from low to high. Greater levels of ME-BSANPs cause an increase in viscosity, which in turn reduces net shear stress and forms

$$Y1 = 254.78 + 44.69X_1 - 25.30X_2 - 8.68X_3 - 1.87X_4 - 19.52X_1 X_2 - 7.45X_1 X_3 - 0.8000X_1 X_4 + 1.43X_2 X_3 - 0.2000X_2 X_4 + 1.28X_3 X_4 + 43.01X_1^2 + 5.65X_2^2 + 1.37X_3^2 + 1.43X_4^2 \quad (2)$$

$$Y2 = -19.90 + 5.17X_1 + 3.78X_2 + 1.12X_3 + 0.4667X_4 - 0.4250X_1 X_2 + 0.6250X_1 X_3 - 0.1000X_1 X_4 - 1.750X_2 X_3 + 0.5750X_2 X_4 - 0.3750X_3 X_4 - 2.05X_1^2 - 0.5083X_2^2 - 0.5833X_3^2 + 0.0292X_4^2 \quad (4)$$

$$Y3 = 0.2640 + 0.2058X_1 + 0.0833X_2 - 0.0575X_3 - 0.0100X_4 + 0.0175X_1 X_2 - 0.0275X_1 X_3 - 0.1025X_1 X_4 - 0.0050X_2 X_3 - 0.0425X_2 X_4 + 0.0050X_3 X_4 + 0.1734X_1^2 + 0.1972X_2^2 + 0.0534X_3^2 - 0.0253X_4^2 \quad (5)$$

The developed model's statistical significance regarding response variables R1, R2, and R3 was established through p-values of <0.0001, <0.0004, and <0.0001, respectively. High response variable R^2 values R1 (0.9844), R2 (0.9820) and R3 (0.9785) indicated a remarkable match between the established polynomial equation and the built model response data. The adjusted R^2 values (0.9950, 0.9640, and 0.9570 for R1, R2, and R3, respectively) and predicted R^2 values (0.9730, 0.9086, and 0.8780) highlighted how well the data suited the created models. ANOVA results presented in Table 4 indicated that the quadratic model demonstrated the best fit for the observed responses, as evidenced by metrics such as R^2 , adjusted R^2 , predicted R^2 , standard deviation (SD), and percent coefficient of variation (% CV) for R1, R2, and R3.

bigger droplets. Moreover, higher viscosity might hinder ME-BSANPs' quick dispersion leading to the development of bigger nanoparticles. Numerous studies consistently demonstrate that nanoparticle size increases with increasing polymer concentration. In this study, PS exhibits a linear decrease with an increase in stirring time, stirring speed, and sonication time (Fig. 8). Fig. 8 shows the 3D response surface for PS with an increase in stirring time, stirring speed, and sonication time are increased. This shows that more mixing energy leads to smaller, less uniform droplets. A noticeable increase in nanoparticle size is observed as the ME-to-ME-BSANPs ratio rises, as shown in Fig. 8. For example, when the ratio is 0.1, the particle size measures 248.3 nm (Run 27). In comparison, a ratio of 1 results in a particle size of 305.4 nm (Run 11). This demonstrates a positive correlation between polymer concentration

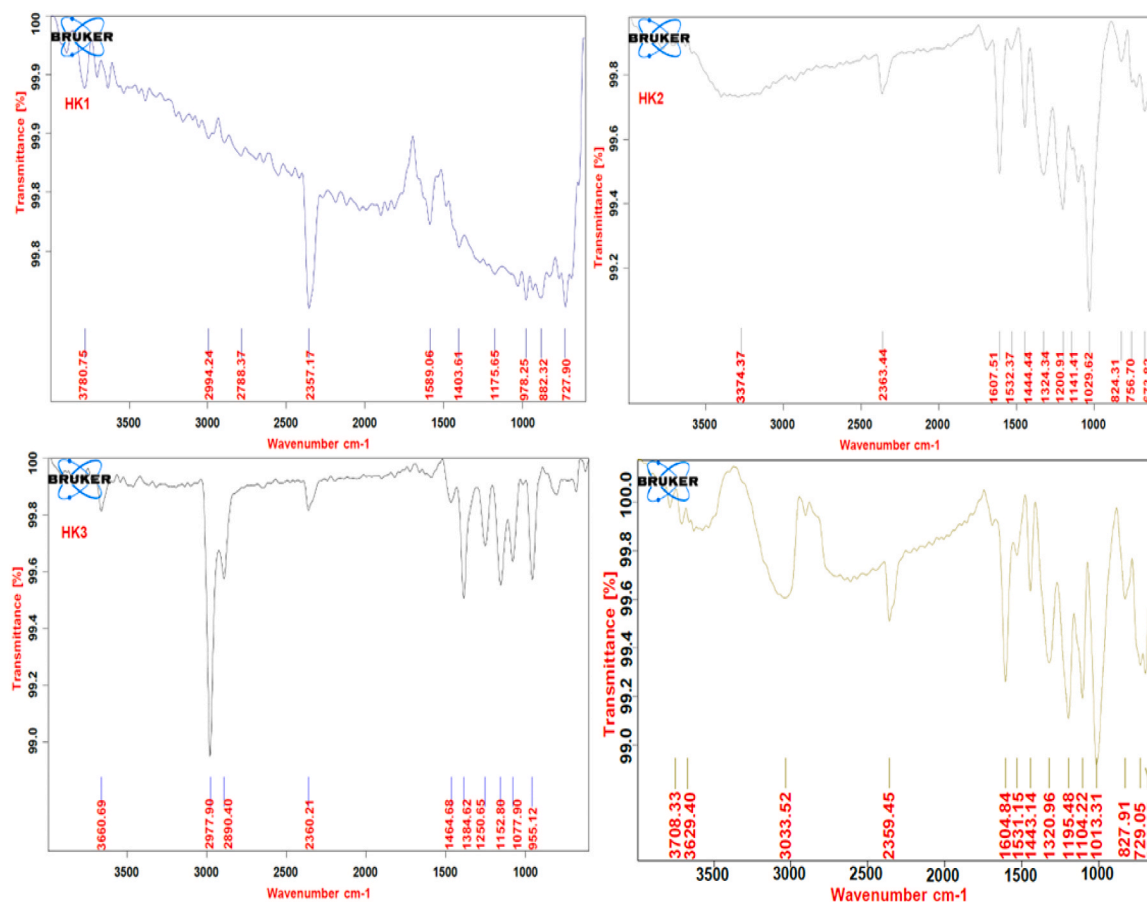


Fig. 5. FT-IR spectra of plain BSA (HK1), methanolic ME bark extract (HK2), physical mixture of ME extract and BSA (HK3) and ME-BSANPs (HK4).

Table 3

FTIR spectra values from ME-BSANPs and methanolic ME bark extract are summarized below, along with an explanation using the sigma IR table.

Wavenumber (cm ⁻¹)	Bond Stretching	Ref. Wavenumber range (cm ⁻¹) (Sigma IR table)	Interpretation
3629.40	O-H	3200–2700	Alcohol–intramolecular bonded
3033.52	O–H	3200–2700	Alcohol–intramolecular bonded
1604.84	C=C	1650–1600	Conjugated alkene
1443.14	S=O	1415–1380	Sulfates, sulfones, or sulfonyl chlorides
1320.96	O=H bending	1390–1310	Phenol
1195.48	C-N	1310–1250	Aromatic amine
1013.31	C–N	1250–1020	Amine
827.91	C=C	840–790	Alkene (trisubstituted)
729.05	C=C	730–665	Alkene (disubstituted)

and particle size (Haider and Soni, 2022). Conversely, increased stirring time leads to a significant reduction in particle size, transitioning from 265.2 nm in Run 5–248.3 nm in Run 27. Similarly, an increase in stirring speed results in a decrease in particle size due to nanoparticle segregation, from 238.4 nm in Run 24–258.9 nm in Run 17. Likewise, increasing sonication time produces a similar effect, and decreasing particle size from 256.4 nm in Run 8–253.5 nm in Run 16 (Zhao et al., 2020).

Colloidal dispersion's stability depends critically on the measurement of the zeta potential of nanoparticles. In this research, nanoparticles made from a mix of ME and ME-BSANPs have a zeta potential that ranges from -13.3 to -32.5 mV (Table 2 and Fig. 9), which is mostly caused by the BSA that is present in the nanoparticles. Conversely, reducing the ME and ME-BSANPs ratios leads to a negative adjustment in the zeta potential values, transitioning from -32.5 in Run 5 to -21.5 in Run 6.

Polydispersity is influenced by the number of polymers used and the

stirring speed. As the concentration of polymer rises, the polydispersity index (PDI) value also rises, going from 0.15 in Run 8–0.89 in Run 11. This is a clear pattern. This increase is associated with nanoparticle aggregation at higher polymer concentrations (Colmenares Roldán et al., 2018). Conversely, increased stirring speed leads to nanoparticle segregation, promoting a more even distribution (Sarmiento et al., 2007). For example, in Run 17, with a stirring speed of 1000 rpm, the Polydispersity Index (PDI) is 0.28. In contrast, Run 8, with a sonication time of 10 minutes, exhibits a lower PDI of 0.16. Moreover, in Run 16, where the sonication time is extended to 30 minutes, the PDI increases to 0.3.

The desirability index, from 0 to 1, signifies the least desirable to the most acceptable combination, ensuring the optimal balance between constraints. Through numerical optimization, the goal is to achieve the target response by applying the desirability function across the experimental domain. The preferred combination is selected based on the desirability function closest to unity, as depicted in Table 5 and Fig. 10.

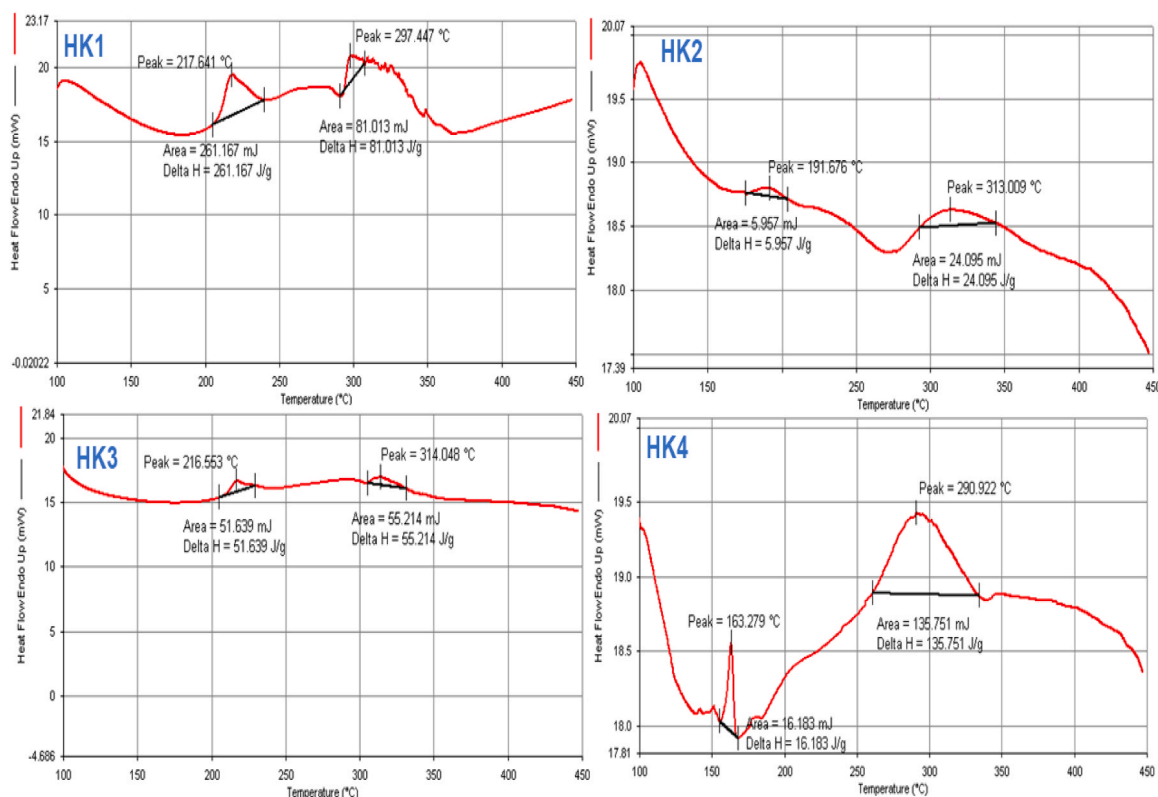


Fig. 6. Differential scanning calorimetry of plain BSA (HK1), methanolic ME bark extract (HK2), physical mixture of ME extract and BSA (HK3) and ME-BSANPs (HK4).

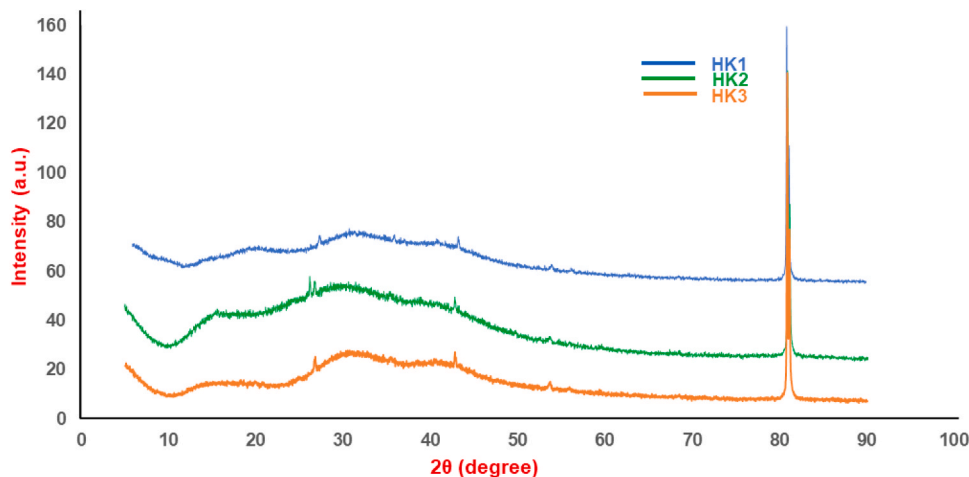


Fig. 7. XRD spectra of plain BSA (HK1), methanolic ME bark extract (HK2), and ME-BSANPs (HK3). The XRD analysis showed the crystalline pattern of the plant material as well as their developed NPs.

Table 4
Design summary and statistics.

Model	Response	R ²	Adjusted R ²	Predicted R ²	SD	%CV
Quadratic	Y ₁	0.9950	0.9900	0.9730	4.09	2.32
Quadratic	Y ₂	0.9820	0.9640	0.9086	0.8422	3.98
Quadratic	Y ₃	0.9785	0.9570	0.8780	0.0418	9.74

The surface contour plot illustrates the interaction of factors on Particle Size (PS). Target values for PS, zeta potential (ZP), and polydispersity index (PDI) during the responses from all 29 formulations serve as the basis for the optimization procedure.

Because Run 1 has the greatest desire of all the formulations, it is determined to be the best-fitting optimum formulation. The optimized formulation exhibits R1 of 229.9, R2 of -17.3, and R3 of 0.52 (Table 1). The requirements for choosing the best-fitting formulation are set at

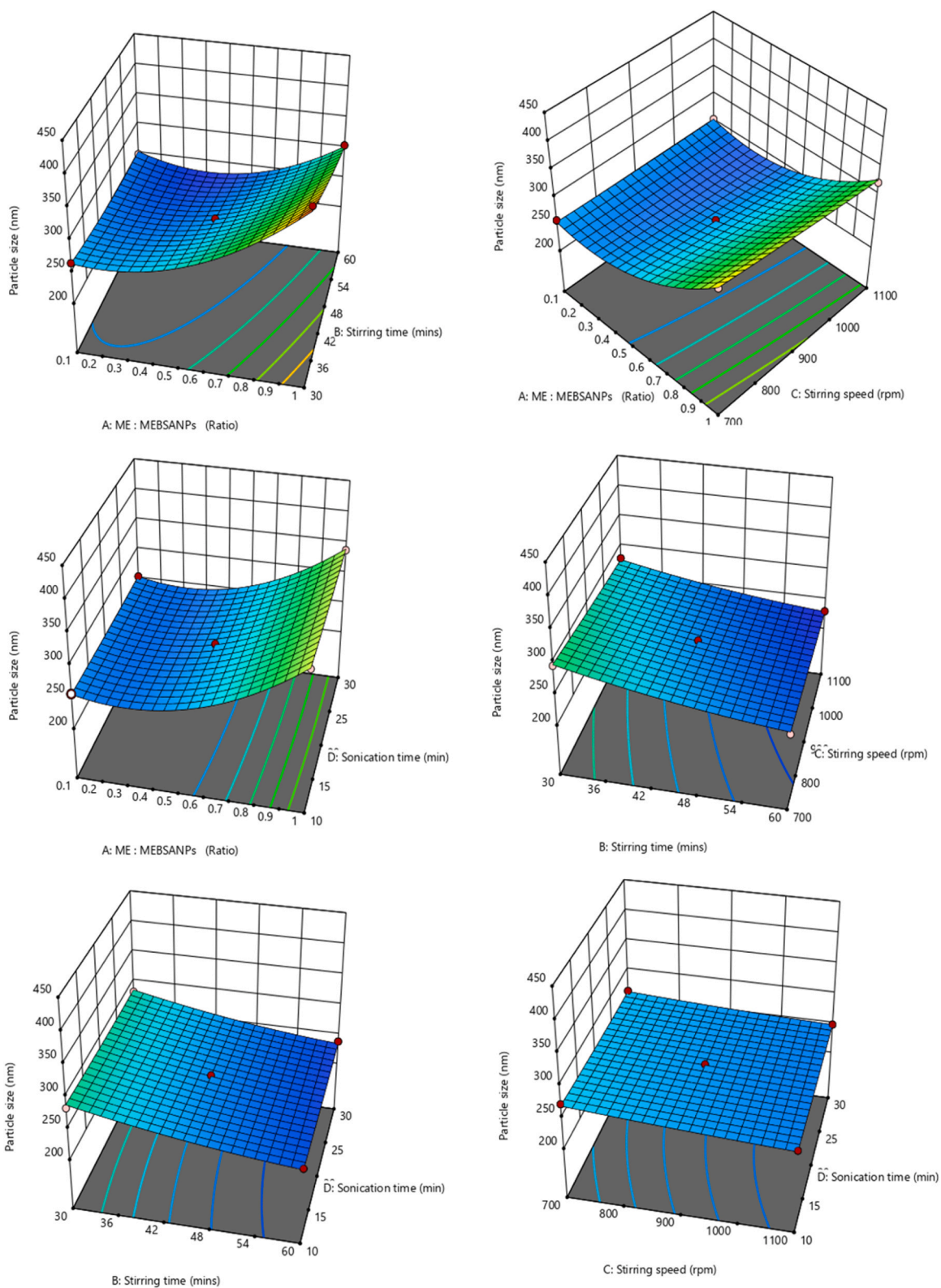


Fig. 8. 3D response surface graphs and contour plots showing relative effects of different independent on particle size.

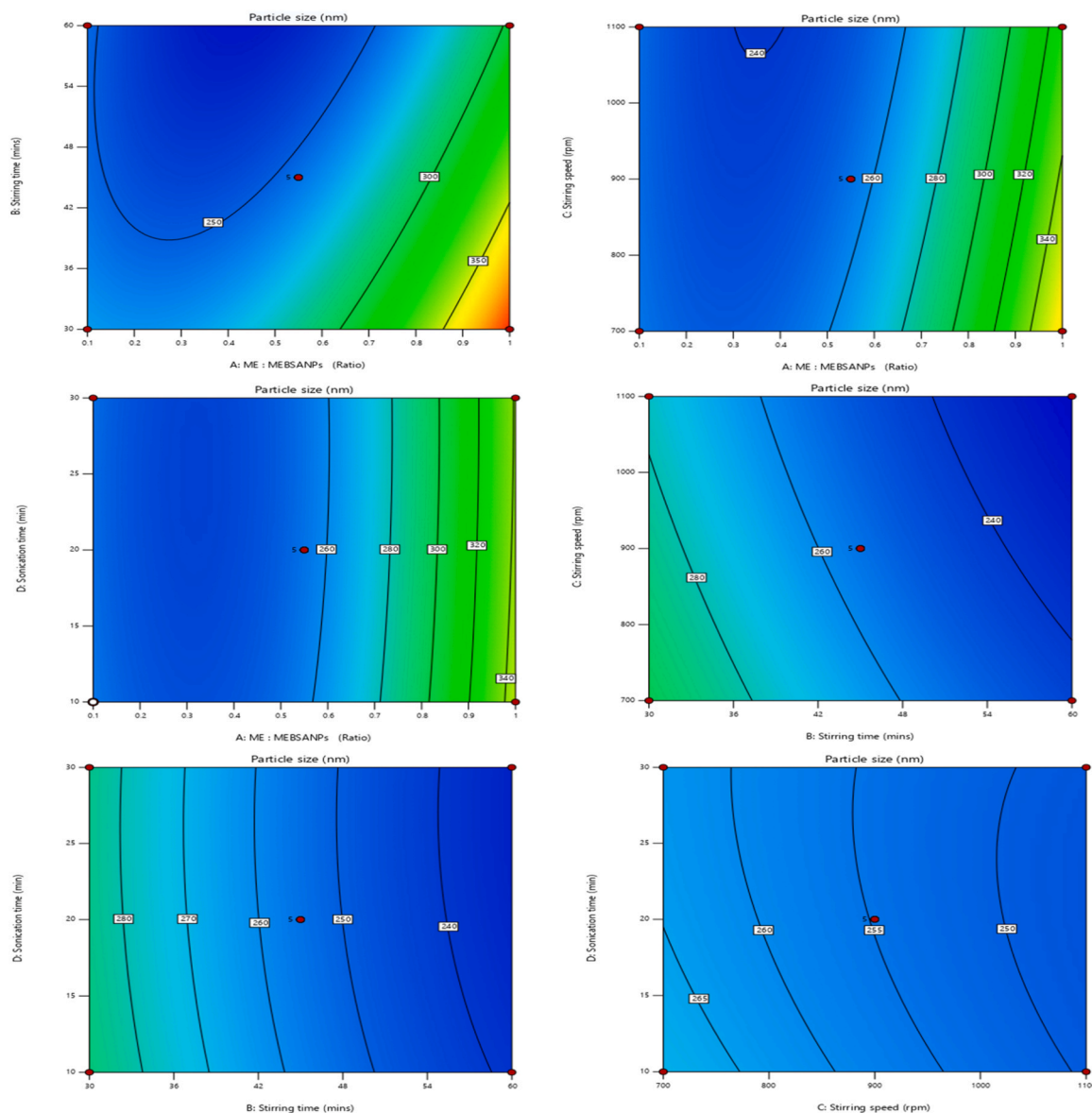


Fig. 8. (continued).

0.55, 60 minutes, 1100 rpm, and 20 minutes for ME: ME-BSANPs, stirring time, stirring speed, and sonication time, respectively. It is discovered that these selection limitations are desirable at 0.99. The best possible nanoparticles with the least amount of particle size (PS), are selected with $R1 = (229.9 \leq R \leq 400.4)$, $R2 = (-32.5 \leq R -13.3)$, and $R3 = (0.16 \leq R \leq 0.9)$ (Table 2). Fig. 11 & 12 display the yellow-colored overlay plot of the design space and show flags that indicate the best places for variables A, B, and C. These design space overlay plots verify that the optimal formulation was chosen from a particular area of the factor space.

3.4. Evaluation of percent cell viability

Cell metabolic activity is measured using the MTT test, which measuring cell viability, proliferation, and cytotoxicity. This test is mostly colorimetric and relies on metabolically active cells reducing a yellow tetrazolium salt (MTT) to purple formazan crystals. The enzymes mitochondrial succinic dehydrogenase and NAD(P)H-dependent oxidoreductase convert yellow MTT to purple formazan in living cells. Using DMSO, acidified ethanol, and sodium dodecyl sulfate in a diluted hydrochloric acid solution, the insoluble formazan crystals are dissolved,

and the colored solution that results is measured using an ELISA plate reader by detecting absorbance at 500–600 nm. The maximum number of viable/metabolically active cells is directly proportional to the darkness of the solution (Vistica et al., 1991; Maehara et al., 1987; Slater et al., 1963).

Using the MTT test, the cytotoxic effects of camptothecin, HK1, and HK2 were examined in MIA Paca-2 cells at a dose of 5 $\mu\text{g}/\text{ml}$ (Fig. 13). After 48 hours, the MIA Paca-2 cells showed $48 \pm 4.2\%$, $40 \pm 3.7\%$, and $58 \pm 2.2\%$ cell growth inhibition for ME NPs, ME-BSANPs, and camptothecin, respectively. The results amply proved that the cytotoxicity of the ME-BSANPs and ME NPs was equivalent. Apart from that, the groups did not receive any treatment referred to as normal control. DMSO ($< 0.2\%$) referred to as solvent control did not show any cytotoxic behaviour against MIA Paca-2 cells. Apart from that, as per the previously published literature, both the extracts MeA (acetone) and MeAA (acidic acetone) were reported to have potent anticancer activities, which led to a 70–92% reduction in the viability of various cancer cell lines such as C33A, SiHa, and HeLa. Also, there was no cytotoxicity was reported in normal cell lines (Saini et al., 2013). Also, the MeOH extract of *Myrica esculenta* screening offered moderate antiproliferative activity against HepG2, HeLa, and MDA-MB-231 cancer cell lines. The MeOH extract

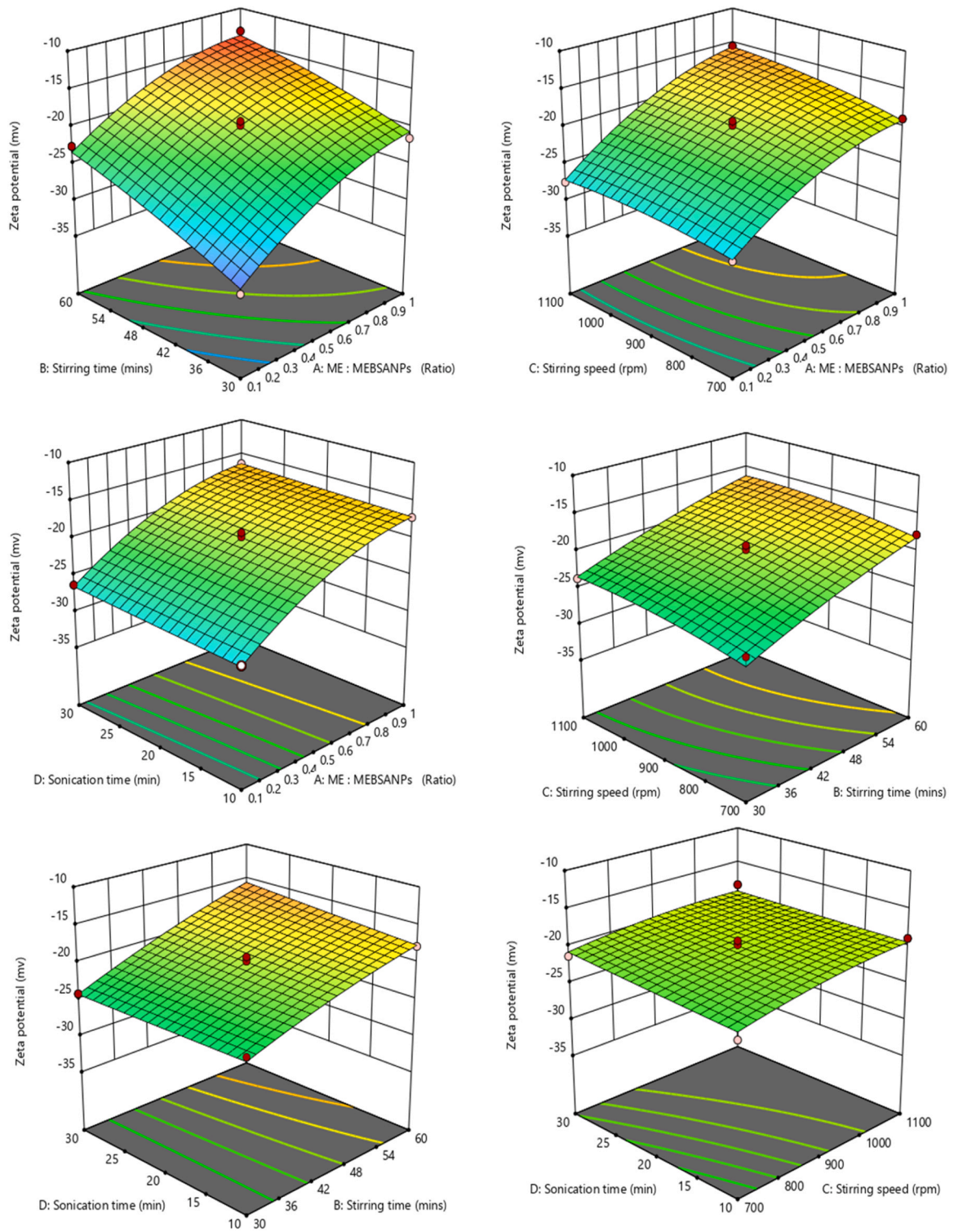


Fig. 9. 3D response surface graphs and contour plots showing relative effects of different independent on zeta potential.

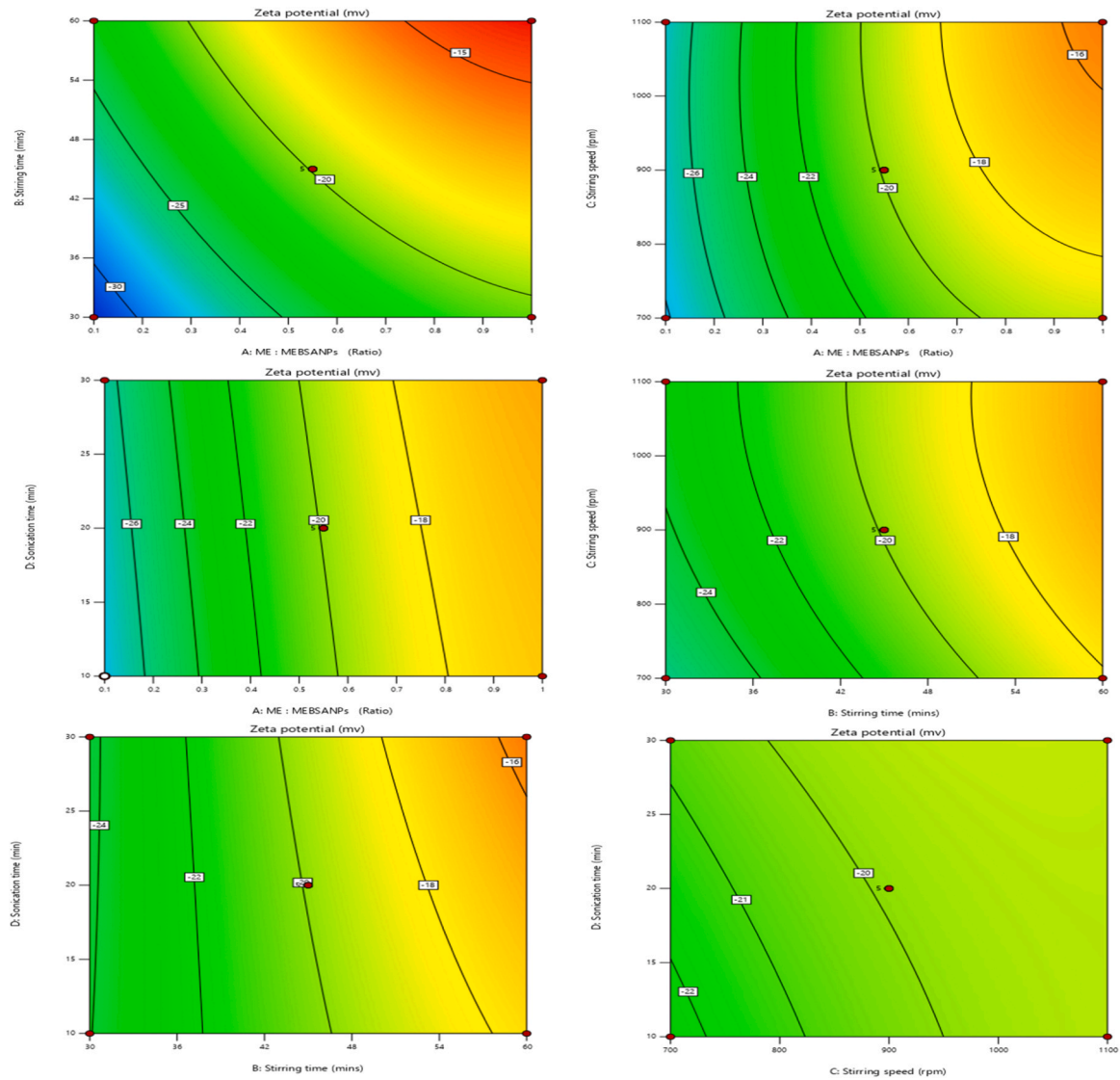


Fig. 9. (continued).

Table 5
Different suggested solutions.

Number	ME: ME-BSANPs	Stirring time	Stirring speed	Sonication time	Particle size	Zeta potential	PDI	Desirability
0.346	0.346	56.330	1099.998	17.010	231.549	-20.000	0.375	0.990
0.346	0.346	56.345	1099.974	17.034	231.549	-20.000	0.376	0.990
0.345	0.345	56.298	1099.995	17.292	231.550	-20.000	0.375	0.990
0.345	0.345	56.384	1099.999	17.137	231.550	-20.000	0.377	0.990
0.344	0.344	56.500	1099.985	16.839	231.550	-20.000	0.379	0.990
0.346	0.346	56.503	1099.990	16.495	231.553	-20.000	0.378	0.990
0.344	0.344	56.692	1099.995	16.478	231.556	-20.000	0.383	0.990
0.343	0.343	56.606	1099.698	16.949	231.557	-20.000	0.382	0.990
0.345	0.345	56.207	1099.726	17.654	231.558	-20.000	0.373	0.990
0.342	0.342	56.751	1099.995	16.786	231.558	-20.000	0.385	0.990

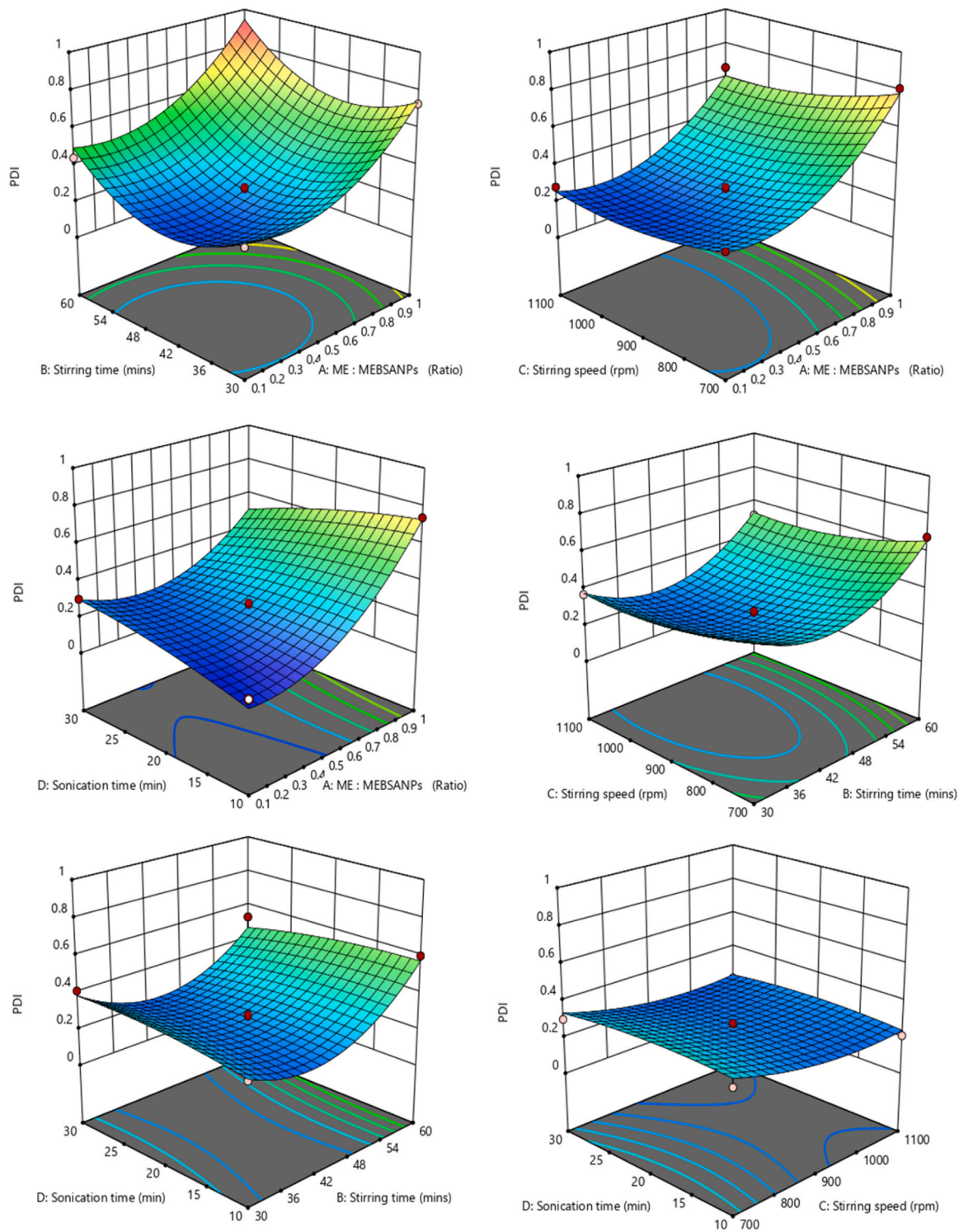


Fig. 10. 3D response surface graphs and contour plots showing relative effects of different independent on PDI.

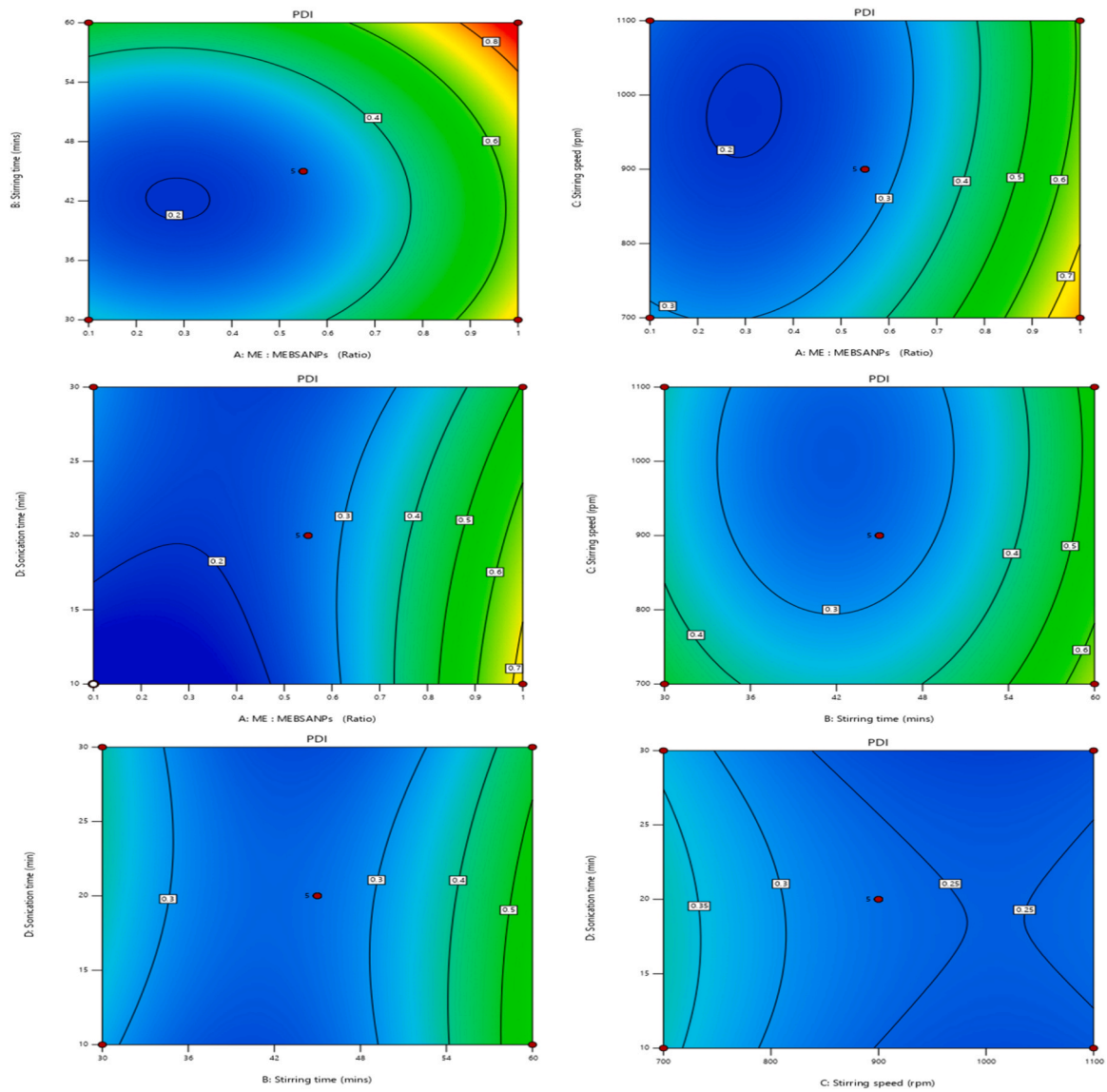


Fig. 10. (continued).

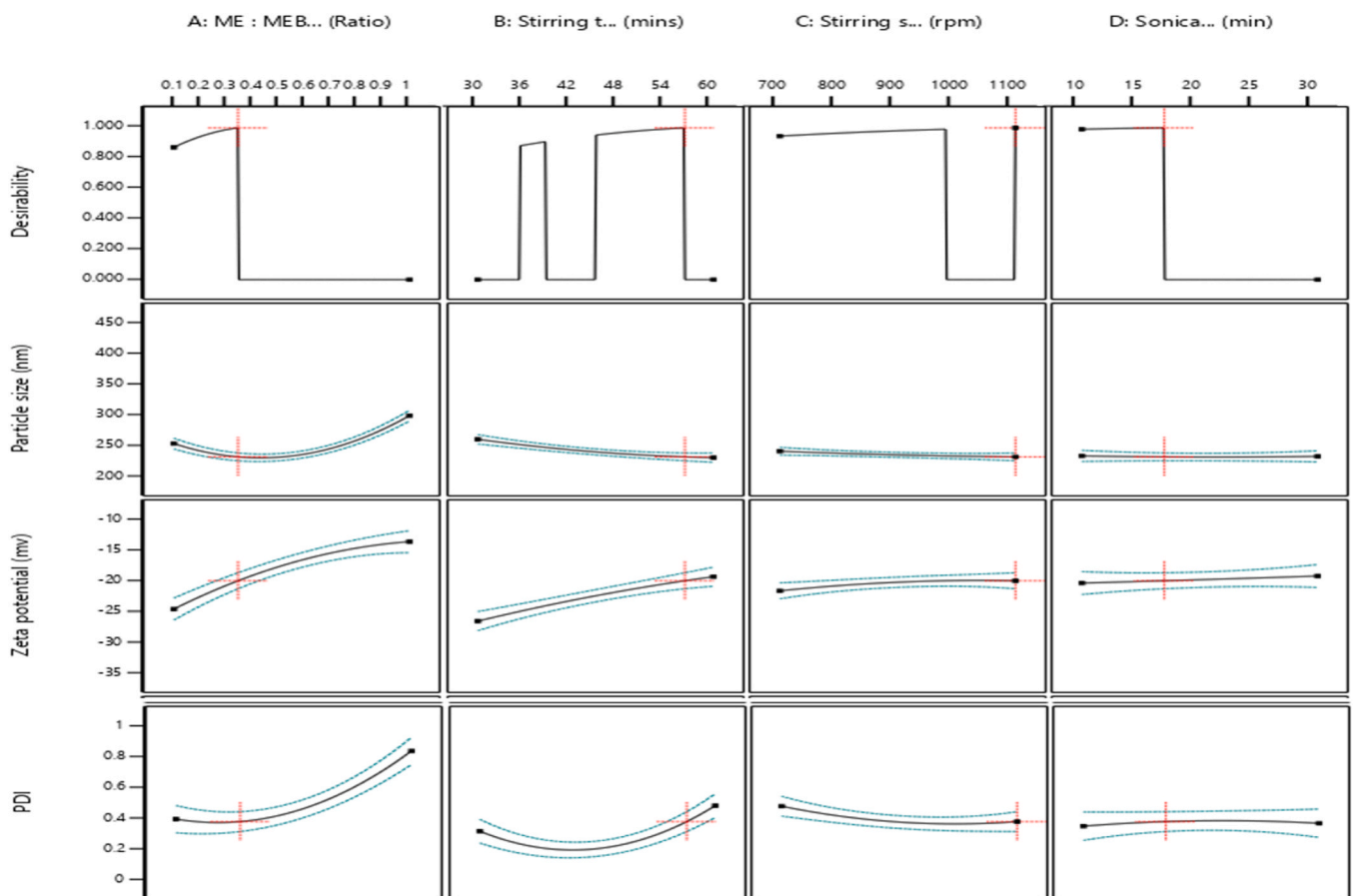


Fig. 11. Desirability plots depicting the independent variables (a) ME: MEBSANPs ratio (b) Stirring time, (c) Stirring speed and (d) Sonication time for producing nanoparticles with the desired targeted responses.

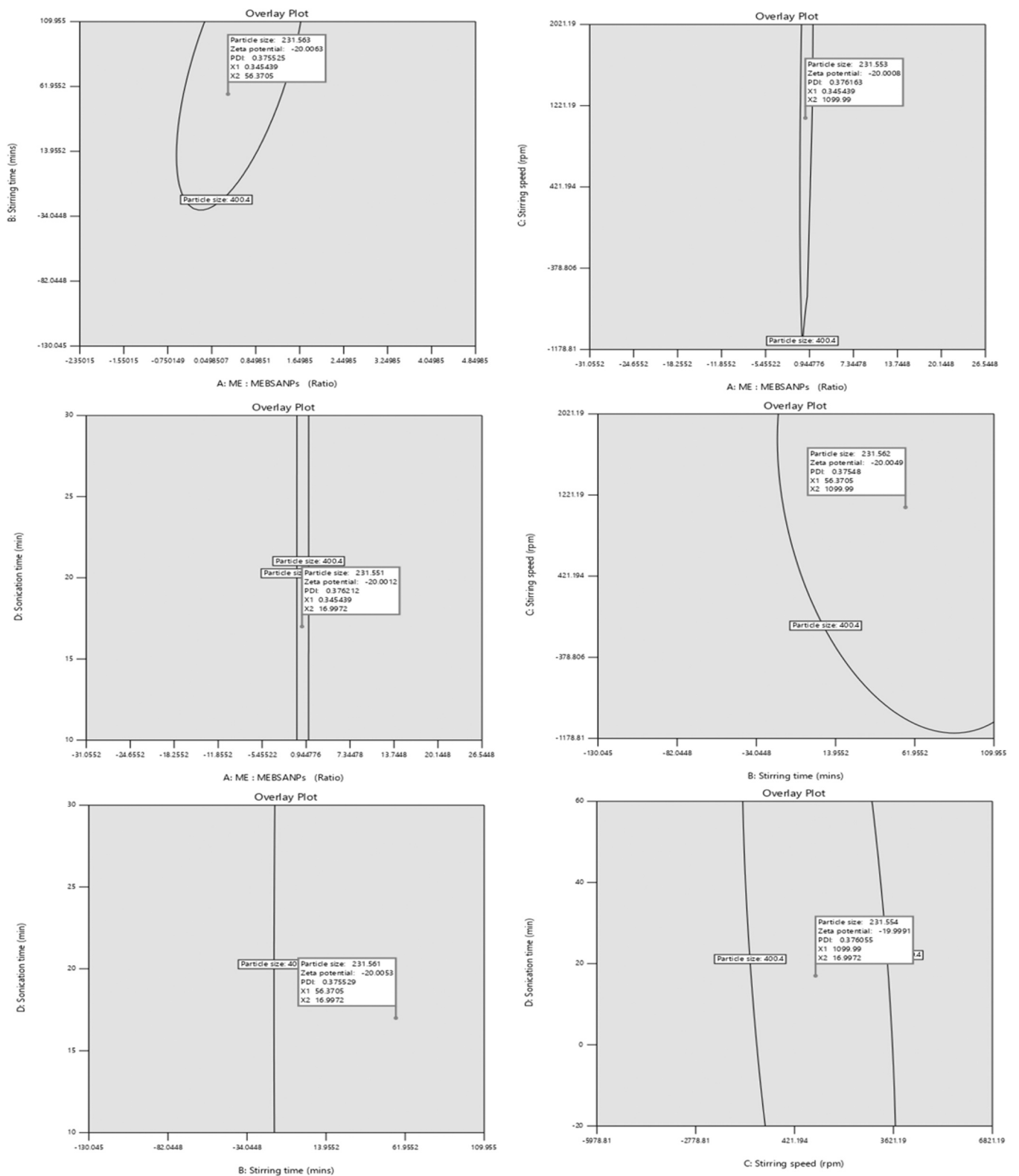


Fig. 12. Design space between (a) ME: ME-BSANPs and stirring speed, (b) ME: ME-BSANPs and sonication time, (c) stirring speed and sonication time.

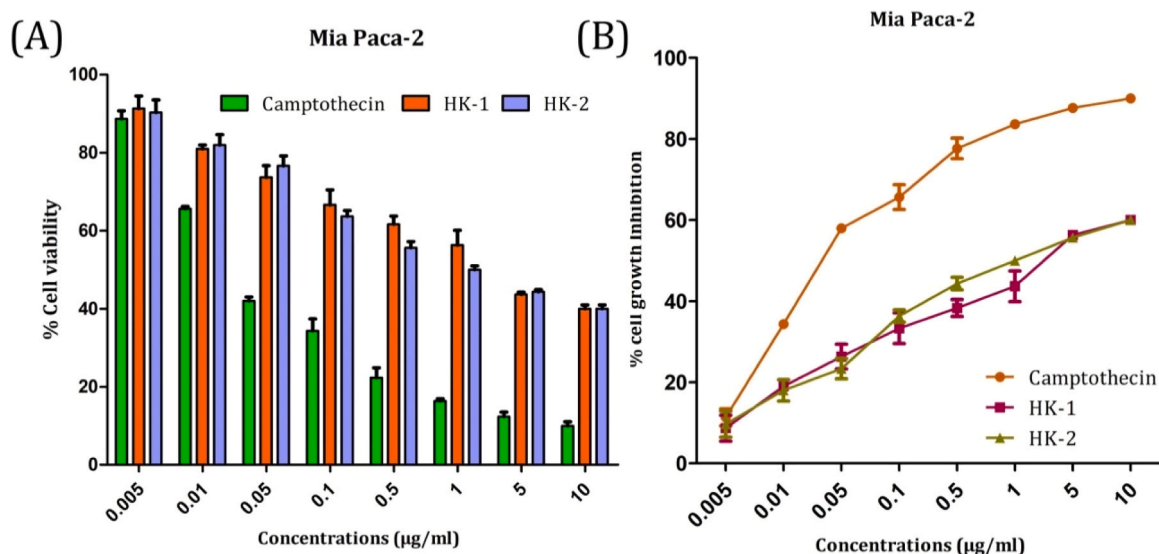


Fig. 13. The cytotoxicity behaviour of ME extract and ME-BSANPs against Mia PaCa-2 cells. (A, B) The cytotoxicity behaviour of ME NPs and ME-BSANPs using MTT assay. Representative image depicting the percentage cell viability and cell growth inhibition at 48 h interval against MIA PaCa-2 cells shows the comparable cytotoxic behaviour of prepared NPs with the plant extract. The cytotoxic behaviour attained might be due to the better inhibitory activity of the developed NPs. Camptothecin was used as a standard positive control in the entire experiment. All data represented as mean±SD, n=3.

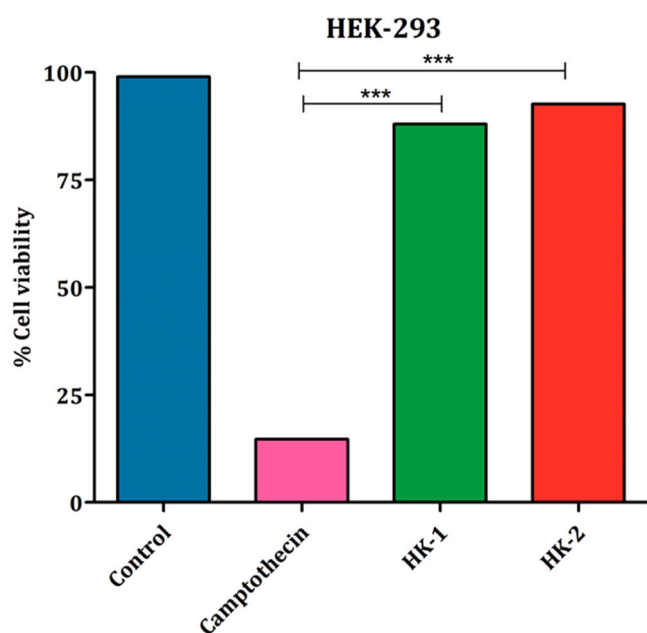


Fig. 14. Representative figure indicated the percentage cell viability of control cells treated with <0.2% DMSO, cells treated with camptothecin, HK-1 and HK-2 at a concentration of 0.65 µg/ml using MTT assay. Compare to camptothecin, HK-1 and HK-2 possessed good number of viable cells count against HEK-293 cells ($p < 0.001$), mean±SD and n =3.

resulted in 46.19%, 50%, and 48.29% inhibition of MDA-MB-231, HepG2, and Hela cells at 5 mg/ml concentration, respectively (Mann et al., 2015) (Mann et al., 2015). Hence, from our study, it was observed that there was an increase in percentage growth inhibition for ME-BSANPs compared to plain ME NPs at the fixed dose of 5 µg/ml concentration, which might be due to the occurrence of bioactive compounds that render the plant serving better anticancer activity.

3.5. Impact on normal cell viability

In this study, HEK-293, human embryonic kidney cell line, was used to assess the effect on normal cell viability. The selected IC₅₀ dose of the formulation HK-2 (0.65 µg/ml) was chosen, and at this dose, camptothecin, plant extract, and formulation (HK-2) were evaluated against normal cells. The results indicated that, the percentage cell viability was not significantly altered in HK-1 and HK-2-treated cells while cells treated with camptothecin triggered cell mortality because of the toxic behaviour of the drug camptothecin (Fig. 14). Both the plant extract and the formulation are found to be selective against Mia PaCa-2 cells while sparing normal (HEK-293) cells. In comparison to camptothecin, the selected IC₅₀ dose of the formulation (0.65 µg/ml) was found to be 5.8-fold (for HK-1) and 6.2-fold (HK-2) safe against normal cells and indicated to be statistically significant ($p < 0.001$). The control cells having <0.2% DMSO did not show mortality compared to normal cells.

3.6. Molecular docking studies

The study of molecular docking interactions showed that different phytochemicals from Myrica esculenta have strong binding affinities for certain amino acid residues on bovine serum albumin (BSA) (Fig. 15). Among the top five compounds with the most favourable docking results were Tannic acid (IMPHY011741), Myricitrin (IMPHY012745), Chlorogenic acid (IMPHY011844), Cianidanol (IMPHY014854), and Myricetin (IMPHY005471). Tannic acid, with a binding energy of -10.163 kcal/mol, formed hydrogen bonds with essential residues such as Glu 52, Tyr 156, Glu 186, Lys 187, Glu 284, Lys 294, and Ser 442, as well as establishing a salt bridge with Lys 187, Arg 217, and a Pi-cat interaction with Lys 280 and Lys 439. Myricitrin, also with a binding energy of -10.163 kcal/mol, demonstrated favourable binding interactions, including hydrogen bonds with Lys 114, Glu 424, Pi-cat interaction with Arg 458, Asp 108, and Pi-Pi interaction with His 145 and Leu 112. Similarly, Chlorogenic acid, with a binding energy of -10.163 kcal/mol, binds with residues Glu 125, Tyr 160, and Ile 181 via hydrogen bonding. Cianidanol, at a binding energy of -10.163 kcal/mol, formed hydrogen bonds with Glu 424, Asp 108, and Leu 112, along with a Pi-cat interaction with Arg 458. Myricetin, with a binding energy of -10.163 kcal/mol, exhibited hydrogen bonding interactions with Leu 346 and Phe 205. These findings provide valuable insights into the

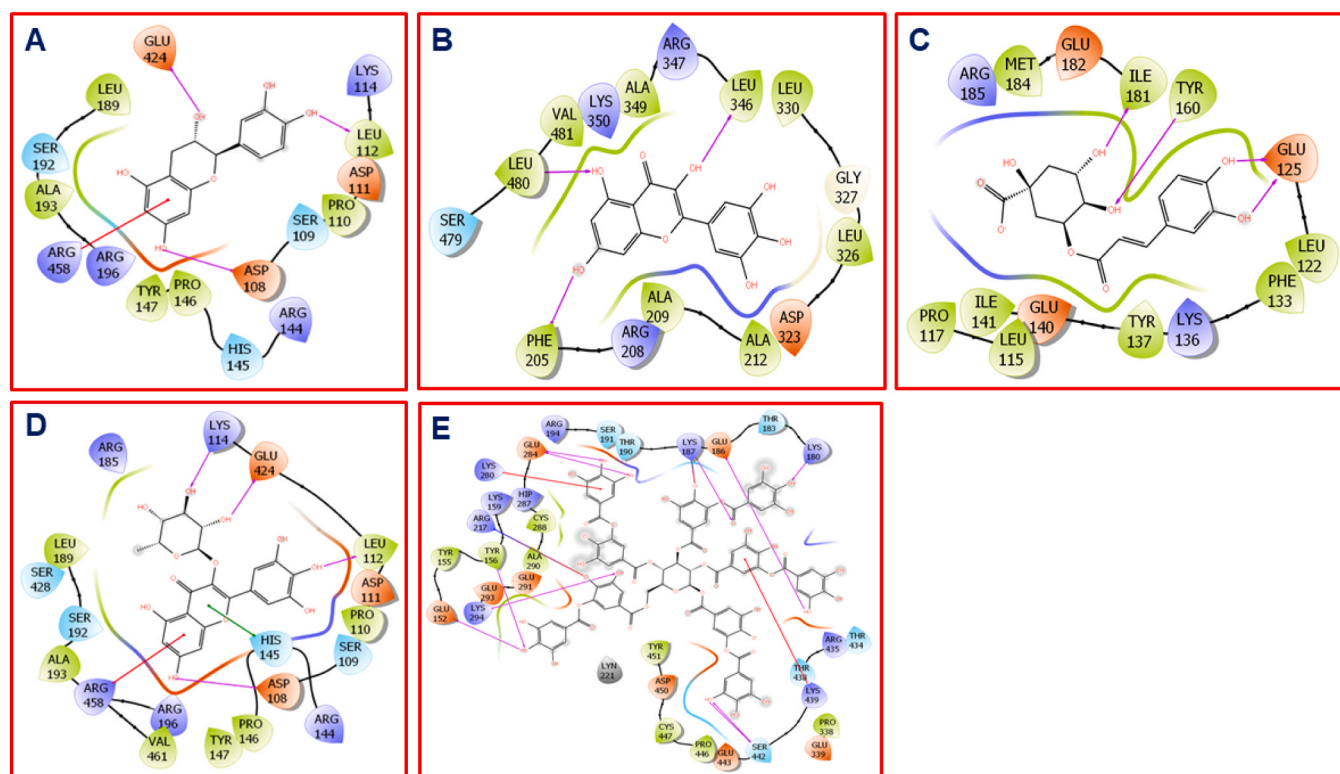


Fig. 15. Investigation of molecular docking interactions and promising binding affinities between various phytochemicals derived from *Myrica esculanta* and specific amino acid residues in BSA. The top five compounds with the most favourable docking results have been shown such as (A) Cianidanol (IMPHY014854), (B) Myricetin (IMPHY005471), (C) Chlorogenic acid (IMPHY011844), (D) Myricitrin (IMPHY012745), and (E) Tannic acid (IMPHY011741).

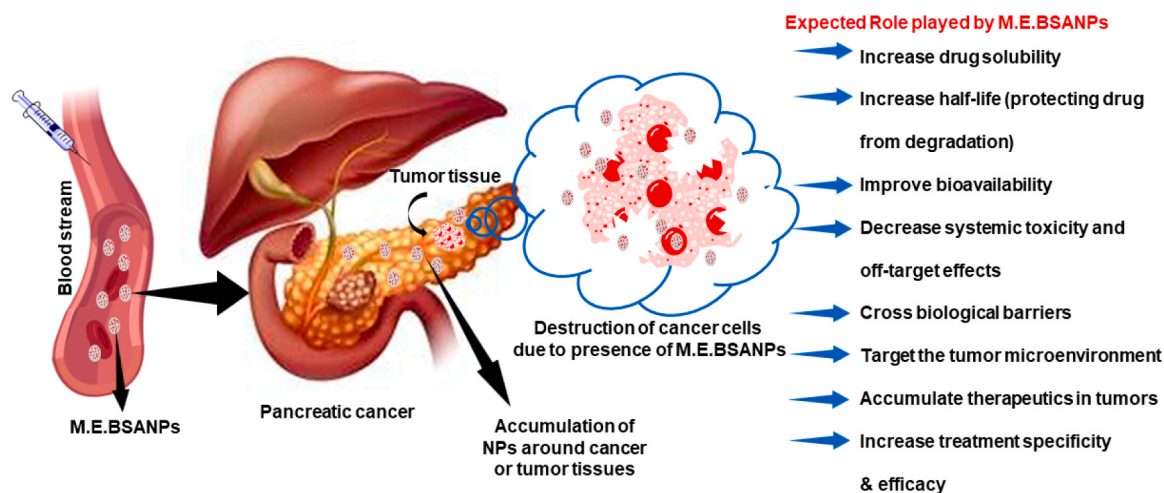


Fig. 16. The advantages of vectorization for the delivery of cancer treatments and its proposed mechanism.

potential molecular mechanisms governing the binding of these phytochemicals to BSA. Furthermore, each of these identified phytochemicals has documented anticancer properties, targeting various proteins associated with cancer, underscoring their potential as agents with anticancer effects. Nevertheless, it is crucial to emphasize the necessity for additional experimental validation to corroborate and expand upon these computational predictions.

3.7. Proposed mechanism

This research project aims to create albumin-based nanoparticles (ME-BSBNPs) from a methanolic bark extract of *Myrica esculanta*. It was

selected as a drug carrier albumin can avoid the reticuloendothelial system (RES) and is non-immunogenic. The authors of this study created and described albumin-based nanoparticles for cancer treatment. This study aims to increase the extract's absorption and cancer cell selectivity. The efficacy and security of nanoparticle drug delivery systems depend on these parameters. The research suggested that these nano-carriers would improve drug solubility and bioavailability, make it easier to target the cancer microenvironment, increase the concentration of drugs in tumors, and make treatment combinations work better (Fig. 16).

4. Conclusion

The current study demonstrated that ME-BSANPs outperformed plant extracts regarding anticancer activity. This could be because the phytoconstituents are delivered more effectively in the methanol extract when there is a concentration. Additionally, the combined effects of methanol extracts and NPs greatly increased NPs' biological potential. This strategy may reduce the negative consequences since BSA is non-toxic, immunogenic, and biocompatible. It also calls for further research in the field of cancer biology. These findings support the use of ME-BSANPs in various biological applications, although further research is required to confirm their efficacy and safety in *in vivo* experiments. Research of this kind would be very helpful in understanding their possible applications in medicine.

CRediT authorship contribution statement

Harsh Kaushik: Writing – review & editing, Methodology, Formal analysis. **Harshita Tiwari:** Writing – review & editing, Formal analysis. **Chittaranjan Behera:** Writing – review & editing, Visualization, Formal analysis. **Rajiv Kumar Tonk:** Writing – review & editing, Methodology, Formal analysis. **Asif Husain:** Writing – review & editing, Visualization, Resources, Formal analysis. **Jay Singh:** Writing – review & editing, Visualization, Resources, Formal analysis. **Kavindra Kesari:** Writing – review & editing, Visualization, Supervision, Funding acquisition, Conceptualization. **Deepak Kumar:** Writing – original draft, Visualization, Supervision, Resources, Project administration, Funding acquisition, Conceptualization. **Monu Kumar Shukla:** Writing – original draft, Methodology, Investigation, Conceptualization.

Declaration of Competing Interest

The authors declare that they have no known competing financial interests or personal relationships that could have appeared to influence the work reported in this paper.

Data Availability

Data will be made available on request.

Acknowledgement

M.K.S. acknowledges the financial support for Shoolini's JRF Fellowship under award no. DF20211654 from Shoolini University, Solan, Himachal Pradesh.

References

- Ahmad, G., Khan, S.U., Mir, S.A., Iqbal, M.J., Pottou, F.H., Dhiman, N., Malik, F., Ali, A., 2022. *Myrica esculenta* Buch.-Ham.(ex D. Don): a review on its phytochemistry, pharmacology and nutritional potential. *Comb. Chem. High. Throughput Screen.* 25 (14), 2372–2386.
- Behera, C., Sandha, K.K., Banjare, N., Malik, S.B., Tabassum, M., Kumar, R., Kumar, A., Mondhe, D.M., Gupta, P.N., 2022 Sep 1. Implication of methylselenocysteine in combination chemotherapy with gemcitabine for improved anticancer efficacy. *Eur. J. Pharm. Sci.* 176, 106238.
- Behera, C., Sandha, K.K., Banjare, N., Shukla, M.K., Ali, S.M., Singh, M., Gupta, P.N., 2024 Jan 5. Biodegradable nanocarrier of gemcitabine and tocopherol succinate synergistically ameliorates anti-proliferative response in MIA PaCa-2 cells. *Int. J. Pharm.* 649, 123599.
- Bhatt, S.C., Kumar, V., Gupta, A.K., Mishra, S., Naik, B., Rustagi, S., Preet, M.S., 2023 Dec 1. Insights on bio-functional properties of *Myrica esculenta* plant for nutritional and livelihood security. *Food Chem. Adv.* 3, 100434.
- Bujacz, A., 2012 Oct 1. Structures of bovine, equine and leporine serum albumin. *Acta Crystallogr. Sect. D: Biol. Crystallogr.* 68 (10), 1278–1289.
- Chauhan, A., Dhatwalia, J., Dutta, V., Gopalakrishnan, C., Rana, G., Hikku, G.S., Kumari, A., Duglet, R., Ghotekar, S., 2023. An investigation of the antimicrobial and antioxidant efficacy of copper oxide (I) nanoparticles: a green approach from *Myrica esculenta* fruit extract. *Chem. Phys. Impact* 7, 100390.
- Chauhan, A., Verma, R., Kumari, S., Sharma, A., Shandilya, P., Li, X., Batoo, K.M., Imran, A., Kulshrestha, S., Kumar, R., 2020 May 12. Photocatalytic dye degradation

- and antimicrobial activities of Pure and Ag-doped ZnO using *Cannabis sativa* leaf extract. *Sci. Rep.* 10 (1), 7881.
- Colmenares Roldán, G.J., Agudelo Gomez, L.M., Carlos Cornelio, J.A., Rodriguez, L.F., Pinal, R., Hoyos Palacio, L.M., 2018. Production of polycaprolactone nanoparticles with low polydispersity index in a tubular recirculating system by using a multifactorial design of experiments. *J. Nanopart. Res.* 20, 1–2.
- Dallakyan, S., Olson, A.J., 2015. Small-molecule library screening by docking with PyRx. *Chem. Biol.: Methods Protoc.* 243–250.
- Das, P.E., Majdalawieh, A.F., Abu-Yousef, I.A., Narasimhan, S., Poltronieri, P., 2020 Feb 15. Use of a hydroalcoholic extract of *Moringa oleifera* leaves for the green synthesis of bismuth nanoparticles and evaluation of their anti-microbial and antioxidant activities. *Materials* 13 (4), 876.
- Dhatwalia, J., Kumari, A., Chauhan, A., Batoo, K.M., Banerjee, A., Radhakrishnan, A., Thakur, S., Guleria, I., Lal, S., Ghotekar, S., Choi, B.H., 2023. *Rubus ellipticus* fruits extract-mediated cuprous oxide nanoparticles: *in vitro* antioxidant, antimicrobial, and toxicity study. *Chem. Pap.* 77 (3), 1377–1393.
- Elzoghby, A.O., Samy, W.M., Elgindy, N.A., 2012. Protein-based nanocarriers as promising drug and gene delivery systems. *J. Control. Release* 161 (1), 38–49.
- Fuku, X., Kaviyarasu, K., Matinise, N., Maaza, M., 2016. Punicalagin green functionalized Cu/Cu₂O/ZnO/CuO nanocomposite for potential electrochemical transducer and catalyst. *Nanoscale Res. Lett.* 11 (1), 2.
- Haider, T., Soni, V., 2022 Sep 1. Response surface methodology and artificial neural network-based modeling and optimization of phosphatidylserine targeted nanocarriers for effective treatment of cancer: *In vitro* and *in silico* studies. *J. Drug Deliv. Sci. Technol.* 75, 103663.
- Hassan, D., Khalil, A.T., Saleem, J., Diallo, A., Khamlich, S., Shinwari, Z.K., Maaza, M., 2018 Oct 31. Biosynthesis of pure hematite phase magnetic iron oxide nanoparticles using floral extracts of *Callistemon viminalis* (bottlebrush): their physical properties and novel biological applications. *Artif. Cells Nanomed. Biotechnol.* 46 (supl), 693–707.
- Kratz, F., 2008. Albumin as a drug carrier: design of prodrugs, drug conjugates and nanoparticles. *J. Control. Release* 132 (3), 171–183.
- Kumari A, Naveen, Dhatwalia J, Thakur S, Radhakrishnan A, Chauhan A, Chandan G, Choi BH, Neetika, Nidhi Antioxidant, antimicrobial, and cytotoxic potential of *Euphorbia royleana* extract-mediated silver and copper oxide nanoparticles. *Chemical Papers.* 2023 Apr 17:1-5.
- Maehara, Y., Anai, H., Tamada, R., Sugimachi, K., 1987. The ATP assay is more sensitive than the succinate dehydrogenase inhibition test for predicting cell viability. *Eur. J. Cancer Clin. Oncol.* 23 (3), 273–276. [https://doi.org/10.1016/0277-5379\(87\)90070-8](https://doi.org/10.1016/0277-5379(87)90070-8).
- Maheshwaran, G., Bharathi, A.N., Selvi, M.M., Kumar, M.K., Kumar, R.M., Sudhakar, S., 2020 Oct 1. Green synthesis of Silver oxide nanoparticles using *Zephyranthes rosea* flower extract and evaluation of biological activities. *J. Environ. Chem. Eng.* 8 (5), 104137.
- Mann, S., Satpathy, G., Gupta, R.K., Sep 2015. *In vitro* evaluation of bio-protective properties of underutilized *Myrica esculenta* Buch.–Ham. ex D. Don fruit of Meghalaya. *Indian J. Nat. Prod. Resour.* 6 (3), 183–188.
- Matinise, N., Fuku, X.G., Kaviyarasu, K., Mayedwa, N., Maaza, M.J., 2017 Jun 1. ZnO nanoparticles via *Moringa oleifera* green synthesis: physical properties & mechanism of formation. *Appl. Surf. Sci.* 406, 339–347.
- O'Boyle, N.M., Banck, M., James, C.A., Morley, C., Vandermeersch, T., Hutchison, G.R., 2011. Open Babel: an open chemical toolbox. *J. Cheminform.* 3 (1), 1–4.
- Petersen, E.F., Goddard, T.D., Huang, C.C., Couch, G.S., Greenblatt, D.M., Meng, E.C., Ferrin, T.E., 2004. UCSF Chimera—a visualization system for exploratory research and analysis. *J. Comput. Chem.* 25 (13), 1605–1612.
- Sackey, J., Nwanya, A., Bashir, A.K., Matinise, N., Ngilirabanga, J.B., Ameh, A.E., Coetsee, E., Maaza, M., 2020 Apr 1. Electrochemical properties of *Euphorbia pulcherrima* mediated copper oxide nanoparticles. *Mater. Chem. Phys.* 244, 122714.
- Saini, R., Garg, V., Dangwal, K., 2013. Effect of extraction solvents on polyphenolic composition and antioxidant, antiproliferative activities of Himalayan bayberry (*Myrica esculenta*). *Food Sci. Biotechnol.* 22 (4), 887–894.
- Sand, K.M.K., Bern, M., Nilsen, J., Noordzij, H.T., Sandlie, I., Andersen, J.T., 2015. Unraveling the interaction between FcRn and albumin: opportunities for design of albumin-based therapeutics. *Front. Immunol.* 5, 682.
- Saneja, A., Kumar, R., Mintoo, M.J., Dubey, R.D., Sangwan, P.L., Mondhe, D.M., Panda, A.K., Gupta, P.N., 2019 May 1. Gemcitabine and betulinic acid co-encapsulated PLGA–PEG polymer nanoparticles for improved efficacy of cancer chemotherapy. *Mater. Sci. Eng.: C* 98, 764–771.
- Sarmento, B., Ribeiro, A.J., Veiga, F., Ferreira, D.C., Neufeld, R.J., 2007 Aug 1. Insulin-loaded nanoparticles are prepared by alginate ionotropic pre-gelation followed by chitosan polyelectrolyte complexation. *J. Nanosci. Nanotechnol.* 7 (8), 2833–2841.
- Shukla, M.K., Parihar, A., Karthikeyan, C., Kumar, D., Khan, R., 2023. Multifunctional QDs for receptor targeting, drug delivery, and bioimaging in pancreatic cancer. *Nanoscale* 15 (36), 14698–14716.
- Shukla, M.K., Behera, C., Chakraborty, S., Sandha, K.K., Goswami, A., Gupta, P.N., 2022. Tumor micro-environment targeted collagenase-modified albumin nanoparticles for improved drug delivery. *J. Drug Deliv. Sci. Technol.* 71, 103366.
- Shukla, M.K., Das, A.K., Gaurav, A., Bisht, D., Singh, A., Kumar, D., 2023. Recent plant-based nanomedicine and nanocarrier for cancer treatment. *Nanotechnology for Drug Delivery and Pharmaceuticals.* Academic Press, pp. 187–206.
- Shukla, M.K., Dong, W.L., Azizov, S., Singh, K.R., Kumar, D., Singh, R.P., Singh, J., 2022. Trends of bioderived carbonaceous materials for futuristic biomedical applications. *Mater. Lett.* 311, 131606.
- Slater, T., Sawyer, B., Sträuli, U., 1963. Studies on succinate-tetrazolium reductase systems. *Biochim. Et. Biophys. Acta* 77383–77393. [https://doi.org/10.1016/0006-3002\(63\)90513-4](https://doi.org/10.1016/0006-3002(63)90513-4).

- Sone, B.T., Diallo, A., Fuku, X.G., Gurib-Fakim, A., Maaza, M., 2020 Jan 1. Biosynthesized CuO nano-platelets: physical properties & enhanced thermal conductivity nanofluidics. *Arab. J. Chem.* 13 (1), 160–170.
- Sood, P., Shri, R., 2018. A review on ethnomedicinal, phytochemical and pharmacological aspects of *Myrica esculenta*. *Indian J. Pharm. Sci.* 80 (1). Jan 1.
- Trott, O., Olson, A.J., 2010. AutoDock Vina: improving the speed and accuracy of docking with a new scoring function, efficient optimization, and multithreading. *J. Comput. Chem.* 31 (2), 455–461. Jan 30.
- Verma, R., Chauhan, A., Kumari, S., Jasrotia, R., Ali, A., Gopalakrishnan, C., Kumar, R., Ghotekar, S., 2023. Green synthesis of ZnO NPs using Timur (*Zanthoxylum armatum* DC.) plant extract for antimicrobial and dye degradation applications. *Chem. Pap. Apr* 18:1-1.
- Vistica, V.T., Skehan, P., Scudiero, D., Monks, A., Pittman, A., Boyd, M.R., 1991. Tetrazolium-based assays for cellular viability: a critical examination of selected parameters affecting formazan production. *Cancer Res* 51 (10), 2515–2520.
- Vivek-Ananth, R.P., Mohanraj, K., Sahoo, A.K., Samal, A., 2023. IMPPAT 2.0: an enhanced and expanded phytochemical atlas of Indian medicinal plants. *ACS Omega* 8 (9), 8827–8845. Feb 23.
- Witjes, J.A., Bruins, H.M., Cathomas, R., Compérat, E.M., Cowan, N.C., Gakis, G., Hernández, V., Espinós, E.L., Lorch, A., Neuzillet, Y., Rouanne, M., 2021. European Association of Urology guidelines on muscle-invasive and metastatic bladder cancer: summary of the 2020 guidelines. *Eur. Urol.* 79 (1), 82–104.
- Xu, J., Kochanek, K.D., Murphy, S.L., Tejada-Vera, B., 2016, Jun 30. Deaths: Final data 2014 65, 4.
- Zhao, Z., Liu, D., Ma, J., Chen, X., 2020. Fluidization of nanoparticle agglomerates assisted by combining vibration and stirring methods. *Chem. Eng. J.* 388, 124213. May 15.
- Zinger, L., Koren, O., Adir, M., Poley, M., Alyan, Z., Yaari, N., Noor, N., Krinsky, A., Simon, H., Gibori, M., Krayem, 2019. Collagenase nanoparticles enhance the penetration of drugs into pancreatic tumors. *ACS Nano* 13 (10), 11008–11021. <https://doi.org/10.1021/acsnano.9b02395>.